# On the timing of retreat of the Loch Lomond ('Younger Dryas') Readvance icefield in the SW Scottish Highlands and its wider significance

John Lowe [1#], Ian Matthews [1], Roseanna Mayfield [1*], Paul Lincoln [1], Adrian Palmer[1], Richard Staff [2 †], Rhys Timms [1]

[1] Centre for Quaternary Research (CQR), Department of Geography, Royal Holloway University of London, Egham, Surrey, UK, TW20 0EX. I.P.Matthews@rhul.ac.uk ; A.Palmer@rhul.ac.u ; Paul.Lincoln@rhul.ac.uk

[2] Oxford Radiocarbon Accelerator Unit (ORAU), University of Oxford, Dyson Perrins Building, South Parks Road, Oxford OX1 3QY

[*]Current address: Department of Geography, Southampton University, University Road Southampton SO17 1BJ. Roseanna.mayfield@gmail.com

[†]Current address: Scottish Universities Environmental Research Centre (SUERC), University of Glasgow, Rankine Avenue, East Kilbride, UK, G75 0QF Richard.Staff@glasgow.ac.uk

# Corresponding author. J.lowe@rhul.ac.uk

**Abstract**

It has long been assumed that the last glacier expansion in the Scottish Highlands, the Loch Lomond Readvance (LLR), resulted from a cold reversal that was broadly coeval with the 'Younger Dryas' episode. This view has recently been challenged, with the suggestion that glacier ice had disappeared from Rannoch Moor, one of the main ice accumulation centres in the SW Scottish Highlands, by as early as 12.5 ka, i.e. within the first half of the 'Younger Dryas'. Here we present new radiocarbon, tephrostratigraphical and pollen-stratigraphical evidence from one of the key sites on Rannoch Moor, the results of an experiment designed to test this hypothesis. Our results not only contradict that concept, but are fully compatible with other evidence from the SW Scottish Highlands that suggests that the LLR glaciers in this area continued to expand until towards the end of the 'Younger

Dryas' period, and may have persisted in some places after the onset of the Holocene. We consider the possible reasons for this marked divergence in chronology, a matter that is crucial to resolve because the precise timing of the demise of the LLR glaciers has important palaeoclimatic and other implications. In the wider context, we also draw attention to problems with the general use of the term 'Younger Dryas' and why we regard the Greenland stratotype unit and term 'Greenland Stadial 1' (GS-1) a more secure stratigraphic comparator.

**Keywords:** Last Termination; Greenland Stadial 1; pollen stratigraphy; radiocarbon dating; tephrochronology; Bayesian-based age models

## 1. Introduction

The final episode of glacier expansion in the SW Scottish Highlands has generally been considered to have been forced by, and hence to have been approximately coeval with, the 'Younger Dryas' cold period (Sissons, 1967, 1974; Gray and Lowe, 1977). This concept has recently been challenged, however, with new evidence interpreted as indicating that both the growth and disappearance of the last glaciers in Scotland took place several centuries earlier than previously supposed (Bromley et al. 2014, 2018; Putnam et al., 2019), a view that has proved controversial. Here we present the results of stratigraphical and chronological investigations designed to test those proposals directly, obtained from a site located in the Rannoch basin, close to the ice divide of the last major icefield to occupy the SW Scottish Highlands. We use this regional example to illustrate (i) the greater chronological finesse and terminological exactitude now required when defining and comparing records dating to the end of the last glacial stage, (ii) why the use of the term 'Younger Dryas' can be problematic and (iii) why we have tended to avoid using this general term in the main body of this article.

The term ‘Younger Dryas’ is frequently used inconsistently in the literature, while lacking precise definition or recognition of its roots. It is most commonly used to denote a specific time interval (the ‘YD chronozone’) or a climatic event (the ‘YD stadial’), but also to refer to particular environmental responses to climatic forcing, for example local glacier or ice sheet expansion (‘YD glaciation’ or ‘YD readvance’). These labels are not, however, universally applicable or interchangeable, for there is growing evidence to indicate that the onset and termination of events previously considered contemporaneous with the ‘YD’ climatic reversal were likely to have been regionally diachronous, even within NW Europe, where the term originated (e.g. Bakke et al., 2009; Lane et al., 2013; Rach et al., 2014).

To complicate matters further, there is no formal international definition for what constitutes the ‘Younger Dryas’. Boundaries for a YD chronozone were proposed by Mangerud et al. in 1974, but these were: (a) tied to the uncalibrated radiocarbon timescale; (b) part of a scheme of stratigraphic classification intended for use in Scandinavia only; and (c) subsequently found to be problematic in their wider geographical application (see e.g. Björck et al., 1998; Walker et al., 1999, 2001; Lowe et al., 2001). An alternative and more secure stratigraphic standard is available, however. The Greenland ice cores offer the best resolved and dated records for the Last Termination, and have provided the template for a North Atlantic regional stratotype sequence spanning the last 120 kyr (Rasmussen et al., 2014). Within this scheme, the pronounced cooling event with which the ‘Younger Dryas’ has generally (but often improperly) been equated is defined as Greenland Stadial 1 (GS-1), with clear lower and upper climatic boundaries indicated by pronounced shifts in multiple proxy indicators, dated by the GICC05 annual ice-layer accumulation chronology to 12.9 ka and11.7 ka b2k (before AD 2000) respectively (Andersen et al., 2006; Rasmussen et al.,

2006; Svensson et al., 2008)[1]. Given that GS-1 is precisely defined and dated with respect to an internationally-recognised stratigraphic type sequence, it offers a more reliable reference standard for comparison purposes than the more equivocal 'YD'.

Used in a chronostratigraphic sense, GS-1 refers to the interval of time between 12.9 and 11.7 ka b2k, but because those boundaries are climatically defined in the Greenland ice cores, this interval also constitutes the GS-1 climatostratigraphic unit *for Greenland*. This does not necessarily apply elsewhere, however. Given the growing evidence for diachronous climatic behaviour across the globe during this interval, the term GS-1 should be employed strictly in a chronostratigraphic sense only when applied to, or compared with, records from areas outside Greenland, where climatic shifts may have led or lagged those in Greenland (Brauer et al., 2014). The *onus* is on the scientific community, therefore, to establish precise climatostratigraphic comparisons with the Greenland stratotype record using independent assessments of the age and duration of local climatic events. This is the approach attempted here, by seeking independent evidence for the timing of the demise of the last glaciers to occupy the SW Scottish Highlands. Before proceeding, however, we outline next the regional palaeo-glacial context, which is crucial for appreciating some of the chronological arguments that follow.

## 2. Limits of the Loch Lomond Readvance (LLR)

The last major ice sheet to cover the whole of Scotland was in significant decline by as early as 19 ka BP, had vacated most of lowland Scotland by ~15 ka BP (Clark et al., 2012),

[1] Ice-core records are dated by counting the number of annual ice-layers that have accumulated prior to the arbitrary datum of AD 2000 (hence b2k). This differs from radiocarbon dates (expressed as $^{14}$C ka BP) and calibrated radiocarbon dates (cal $^{14}$C ka BP) for which the datum is 1950 CE. The datum for surface exposure ages (expressed as ka BP) is the year in which the measurements were made.

and was confined to the western Highlands by ~14 ka BP (Ballantyne and Small, 2019; Walker and Lowe, 2019). There is convincing evidence for a readvance of the receding ice-sheet margin shortly before 15 ka BP, but evidence for this appears to be restricted to NW Scotland (Ballantyne and Stone, 2012). Post-14 ka BP, the ice sheet continued to shrink into the most favoured upland locations, but whether some vestigial remnants survived until conditions favoured renewed growth, or glacial ice disappeared from Scotland completely, remains unclear (Ballantyne and Small, 2019). After this, however, the glaciers re-expanded to reach some limits beyond the Highland margins (**Figure 1)**, first demonstrated from stratigraphical evidence in the vicinity of the southern shore of Loch Lomond by Simpson (1933), but studied in greater detail by Rose (1981) in what is now the type locality for this phase of glacier activity, termed the Loch Lomond Readvance (LLR). The reconstructed glacier limits represented in **Figure 1** are based on extensive mapping of a range of glacigenic landforms and sediments, including the distribution of well-defined morainic or other glacigenically formed mounds (in older literature commonly and collectively referred to as 'hummocky moraine') and/or prominent terminal moraines or other ice-marginal features, such as outwash fans and deltaic sequences. Overviews of the collective geomorphological evidence on which the empirical ice limits are based can be found in (*inter alia*) Sissons (1974), Sutherland (1984), Benn (1997), Golledge (2010), Bickerdike et al. (2016, 2018a, 2018b) and Chandler (2018).

That LLR ice expanded beyond the margins of the Scottish Highlands is demonstrated in two principal ways. First, redeposited marine shells can be observed in exposed terminal deposits of the LLR at several outlets along the western seaboard and in the arcuate terminal deposits that enclose the Loch Lomond and Menteith basins (**Figure 1**). As the ice advanced into these locations, it over-rode marine sediments laid down during the preceding Late-

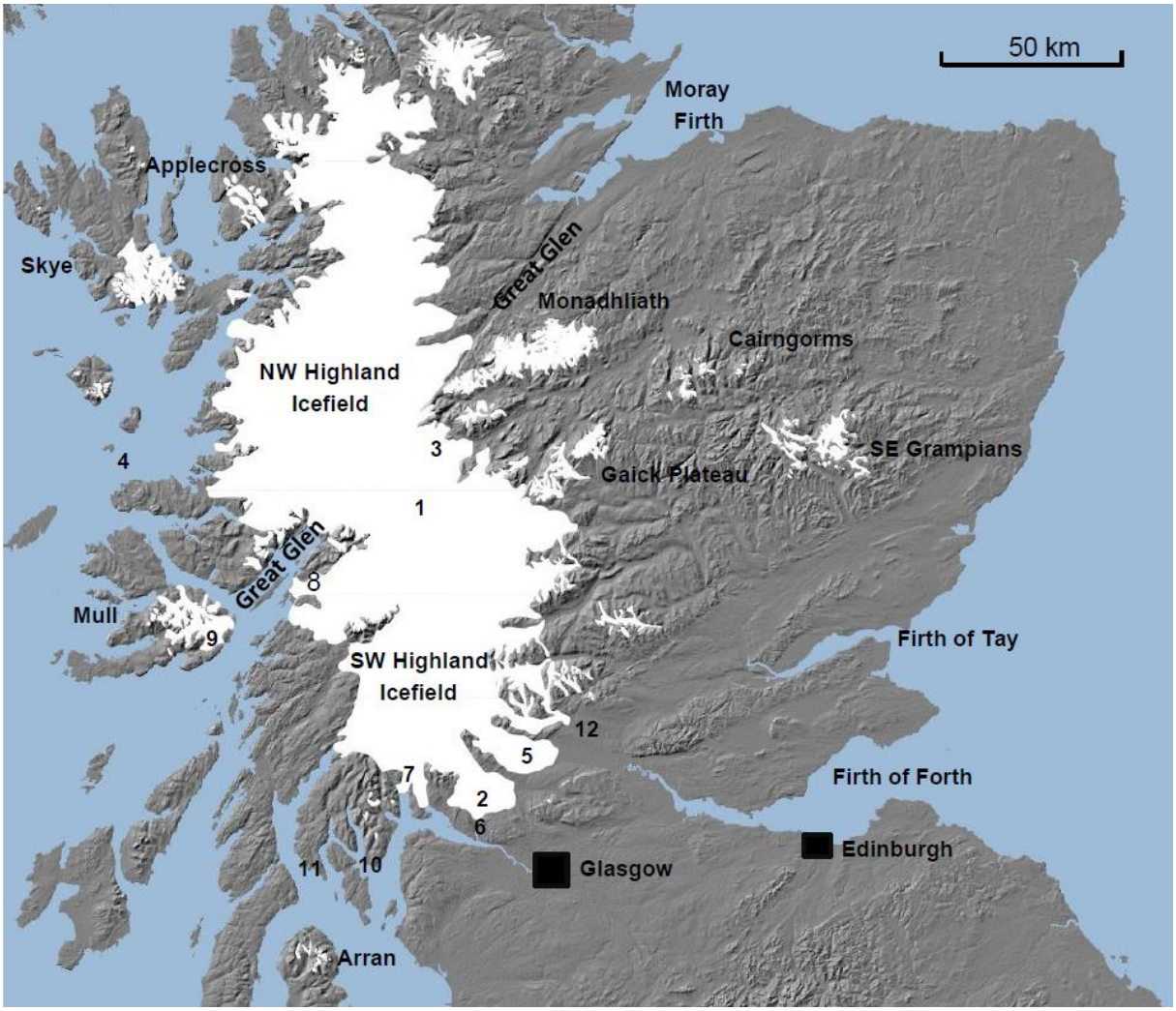


**Figure 1.** The maximal glacial limits of the Loch Lomond ('Younger Dryas') Readvance in mainland Scotland and the Inner Hebrides (based on Chandler 2018; Chandler et al., 2019). Also indicated are locations mentioned in the text, including: 1. Rannoch basin; 2. Loch Lomond basin; 3.Glen Spean-Glen Roy area; 4. the Muck Deep; 5. the Menteith basin; 6. Balloch/Inverleven; 7.Loch Goil; 8. Loch Creran; 9. Kinlochspelve; 10. Ardyne; 11. Portavadie; 12. the Teith Valley.

glacial Interstadial (GI-1), incorporating some of the material, including fragmented or entire marine shells, into tills and other sediments subsequently deposited at or near the glacier margins. Radiocarbon dates based on these transported shells, obtained for example from Loch Lomond and Menteith (Sissons, 1967; Rose, 1981), Kinlochspelve (Gray and Brooks, 1972), Loch Creran (Peacock 1971; Peacock et al., 1989), Balloch/Inverleven (Browne and Graham, 1981), Loch Goil (Sutherland, 1981) and Portavadie and Ardyne (Peacock et

al.,1978; Sutherland 1986), and additional dates obtained more recently from some of these sites by Bromley et al. (2018), suggest that they generally date to between ~14.5 and ~12.6 cal $^{14}$C ka BP, when calibrated using IntCal13 (Reimer et al., 2013). Hence the readvance, at least when the glaciers were nearing their maximal limits, post-dated this time interval. Second, in some places *in situ* terrestrial organic deposits are preserved beneath LLR glacigenic deposits, for example in the Loch Lomond basin (Rose et al.,1988; MacLeod et al. 2011) and the Teith Valley (Merritt et al. 1990), showing that they were buried by the advancing LLR ice. The precise timing of the onset of the readvance, and of when the glaciers reached their maximal limits and subsequently began to retreat are, however, matters of considerable debate (see e.g. Ballantyne, 2012; Small and Fabel, 2016a; 2016b; Bromley et al., 2016; Peacock and Rose, 2017; Palmer and Lowe, 2017). Here we focus only on evidence for the timing of the demise of the LLR in the SW Highlands; the other topics will be addressed in separate contributions.

The new evidence we will present was obtained from a site on Rannoch Moor, the area from which Bromley et al. (2014) obtained the data on which their interpretations were based. Rannoch Moor is an extensive area of boggy moorland (~130 km$^2$) that covers part of a major topographical basin, the latter an artefact of the region's complex orogenic and erosional history. The floor of the basin is underlain by an intrusive igneous complex composed mostly of granodiorite and granitic rocks of Siluro-Ordovician age, emplaced ~422 million years ago (Nielson et al., 2009). The basin is surrounded on three sides by high mountains composed of older metamorphosed Dalradian metasediments, which underpin most of the Grampian Mountains (Stephenson et al., 2013). Throughout this paper we refer to Rannoch Moor when considering the peatland records from which stratigraphical and

chronological evidence was obtained, and to the Rannoch basin when considering the larger topographical setting which encompasses the moor.

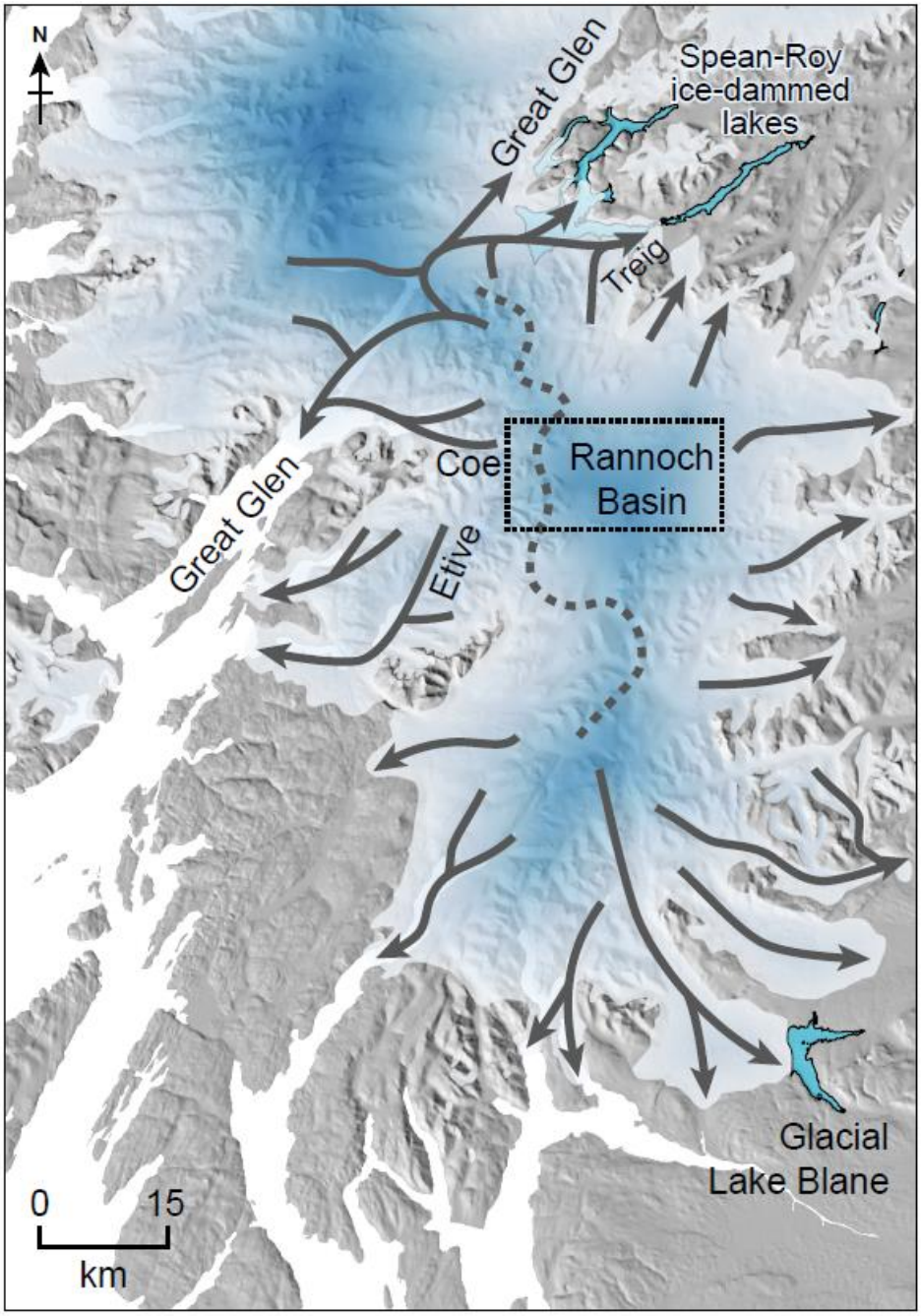


**Figure 2.** Schematic representation of the principal ice-flow lines (arrows) of the SW Highland icefield (blue-white shading), based partly on the results of numerical modelling of Golledge et al. (2009), which indicate that fast ice-streams feeding the major outlets reached velocities of up to 126 m $a^{-1}$. The dotted line shows the position of the main ice shed (after Thorp, 1991). The valleys of Glen Coe and Glen Etive are named as they are labelled in Figures 3 and 4 for orientation. The dotted rectangle shows the approximate limits of the mapped area in Figure 3.

It is important to appreciate the palaeoglacial significance of the Rannoch basin when assessing the stratigraphical and chronological information that is discussed later, for it served as one of the principal source areas for growth of the SW Highlands icefield during the LLR, fed mainly by the mountains along its western margin, in the vicinity of Black Mount (**Figure 3**). Numerical modelling of ice-flow velocities generated by the SW Highland icefield at its maximum extent reflect the importance of a number of prominent arterial ice streams that radiated from a principal ice shed that extended southwards from the western part of the Rannoch basin (**Figure 2**), a dynamic ice-flow pattern previously also inferred from empirical data (e.g. Sissons 1967; Sutherland, 1984; Thorp, 1991). The records referred to in the following sections were obtained from sites located on or close to this ice shed, in the western margin of Rannoch Moor (**Figure 2**).

## 3. Contradictory proposals for the timing of the demise of the SW Highland icefield

At the height of the LLR the Rannoch basin was covered by an ice cap with an estimated surface elevation of 900 m, the thickness of the ice cover exceeding 450 m in places (Thorp, 1991; Golledge, 2007). As the ice margin retreated it deposited a complex series of linear or irregular boulder-strewn recessional moraines (**Figure 3**), which in places enclose small depressions that have subsequently become infilled: some of the deeper depressions (up to ~7 m below local ground surface) initially accumulated lake sediments (gyttja or lake muds) now buried beneath blanket peat (example shown in **Figure 4**). The geomorphological evidence suggests the ice retreated in an approximately NE to SW direction, back towards the main local ice source area in the vicinity of Black Mount.

In a first attempt to constrain the timing of local deglaciation in this area at the end of the LLR, Lowe and Walker obtained a series of radiocarbon dates from the lowermost

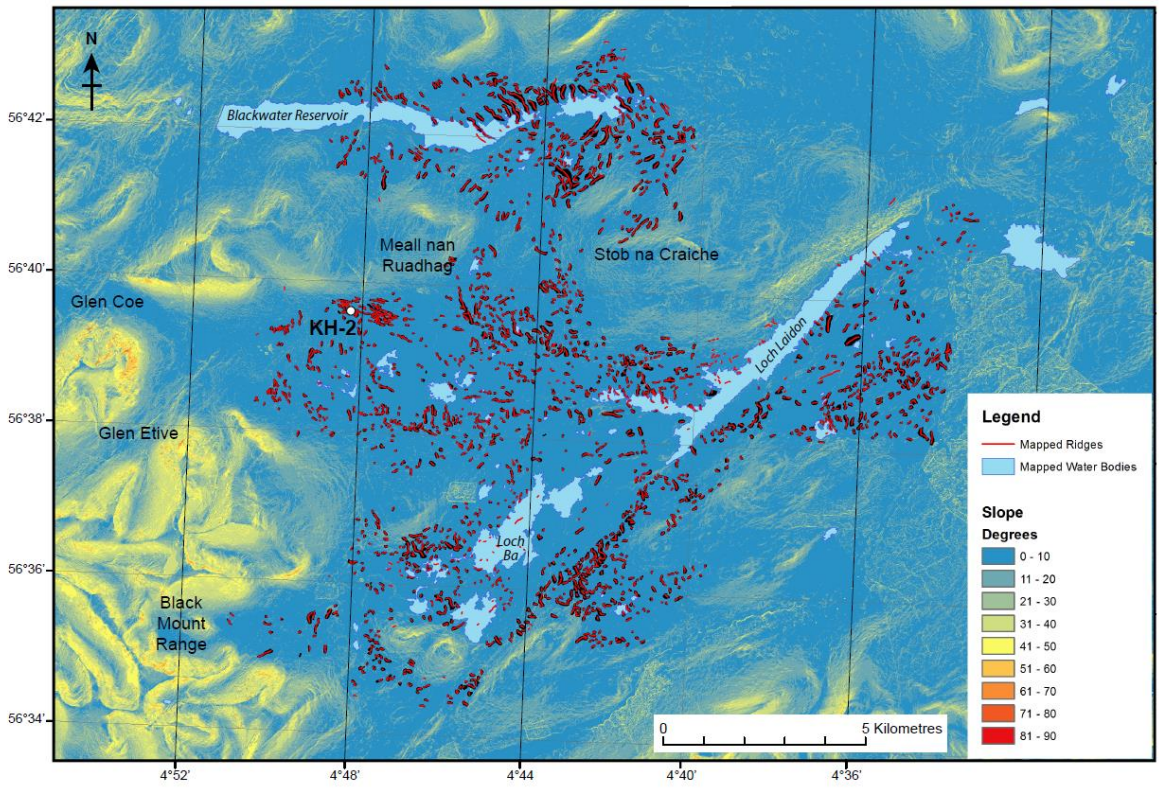


**Figure 3.** Distribution of irregular moraine mounds and linear recessional moraine ridges (both in red) of Loch Lomond Readvance age in the western part of the Rannoch basin: the dashed rectangle in Figure 2 shows the location of the area represented. The topographical map is based on the interpretation of NEXTMap Britain elevation and slope gradient data (colour coded in the legend in degrees) supplied by Intermap Technologies in collaboration with the British Geological Survey (Natural Environment Research Council, UK) and reproduced from Hornsey (2016). The green dot marks the location of the Kingshouse 2 site (KH-2).

organic sediments preserved in several depressions located on or adjacent to Rannoch Moor (Lowe and Walker 1976, 1979; Walker and Lowe 1977, 1979, 1981). However, all of the dates they obtained, with one exception, were based on bulk sediment samples which are prone to inbuilt age errors caused either by assimilation of inert carbon originating from fine-grained carbonaceous particles within the sediment matrix, or *via* photosynthesis by aquatic plants in calcareous water (see Lowe and Walker 1979, 1980, 2000). The exception was a date based on a 2-cm thick layer of the moss *Racomitrium lanuginosum* (woolly fringe


**Figure 4.** The Kingshouse 2 basin (located at western margin of Rannoch Moor) in foreground, enclosed by moraine ridge of LLR age (on which figure is seated). The rods protruding from the peat surface mark the locations of the boreholes from which basal cores were recovered (see **Appendix A**). Photographs of two of the basal cores are shown as insets, and exemplify the consistency of the basal lithostratigraphic units, comprising from base: L1. Sands and silts. L2. Prominent moss layer, dominated by remains of *Racomitrium lanuginosum*. L3. Silty sands, with occasional moss bands. L4. Silty-clays with more abundant moss bands. L5. Organic muds grading into peat.

moss) discovered near the base of the sediment infill of the site named Kingshouse 2 (**Figure 4**) and which, at the time, was believed to be wholly terrestrial in habitat; this yielded a radiocarbon date of 10.29 ± 180 $^{14}$C a BP, with a calibrated age range at 95% probability of 12.59 -11.39 $^{14}$C cal ka BP (using IntCal13; Reimer et al, 2013). A bulk gyttja sediment sample from below the *Racomitrium* layer yielded a radiocarbon age of 10.52 ± 330 $^{14}$C ka BP (13.04 -11.33 $^{14}$C cal ka BP), but because of the aforementioned inbuilt age problems, greater credence was afforded to the moss date as the more reliable index of the timing of local deglaciation. This led Lowe and Walker (1976) to conclude that Rannoch Moor became

ice-free before ~10.2 $^{14}$C ka BP (between ~12.59 and ~11.36 $^{14}$C cal ka BP when recalibrated using IntCal13).

More recently, Bromley et al. (2014) collected basal sediment cores from 8 basin sites located in the western sector of Rannoch Moor, from which a total of 32 radiocarbon dates were obtained, most of which were considered to be based primarily on terrestrial plant macrofossils (a claim we dispute in section 5.2 below). The ages obtained ranged from 9.14 ± 180 to 10.55 ± 65 $^{14}$C ka BP, which they calibrated to between ~10.32 and ~12.48 $^{14}$C cal ka BP. On the basis of their results, Bromley et al. (2014) concluded that the earliest probable age for plant colonisation of the western sector of Rannoch Moor was ~12.48 $^{14}$C cal ka BP, and that deglaciation of the Rannoch basin was probably complete by as early as ~12.58 $^{14}$C cal ka BP, and no later than ~12.20 $^{14}$C cal ka BP. This led them to speculate about the possible climatic forcing factors that may have led to this part of Scotland becoming ice-free in the middle of the 'Younger Dryas'.

Small and Fabel (2016a) estimated the timing of the deglaciation of the Rannoch basin by measuring $^{10}$Be/$^{9}$Be ratios of the surfaces of granite boulders resting on the crests of moraine ridges adjacent to some of the basin sites investigated by Bromley et al. (2014); the resulting exposure ages range from 12.83 ± 0.68 to 11.29 ± 0.59 ka BP, giving a collective range at 68% confidence of 13.51 to 10.70 ka and a computed best-estimate mean age of 11.5 ± 0.6 ka. Small and Fabel therefore concluded that deglaciation of the Rannoch basin did not occur until towards the end of the LLS or possibly after the onset of the Holocene. Following the publication of these results, Bromley et al. (2016) and Small and Fabel (2016b) exchanged critical assessments of each other's results, which served to illuminate areas of uncertainty associated with each of the dating methods employed, a matter we return to later.

In light of these significantly discordant age estimates for the timing of the deglaciation of the Rannoch area, we re-investigated the basal sediment sequence preserved in the Kingshouse 2 site in an attempt to resolve the matter. The aims of this study were to test the integrity of radiocarbon dates previously obtained from small lake basins on Rannoch Moor by (a) obtaining a new series of radiocarbon dates with closer scrutiny of any bias relating to the nature of the dated material; (b) constraining the dated samples stratigraphically; and (c) exploring the possibility of detecting cryptotephra layers, which might offer the potential for independent validation of the radiocarbon results. The results obtained from this experiment are presented next.

## 4. New evidence from the site of Kingshouse 2, western Rannoch Moor

### *4.1 Stratigraphy*

Several basal cores were collected from the Kingshouse 2 site (56°39′35″ N; 4°48′12″W; grid reference NN 2823 5551) in 2015 and **Appendix A** provides images and lithological descriptions for five of the recovered cores. Although there are some minor differences between them, the basal layers are consistent in showing the five clear basal lithostratigraphic units that are illustrated and numbered in **Figure 4**, with distinctive boundaries that aid core correlation. Pollen-stratigraphic, radiocarbon and tephrostratigraphical data were obtained, using the methods described in **Appendix B**.

The lowermost minerogenic sediments in the sequence (lithological units (l.u.) 1 and 2; **Figure 5**) contained such sparse pollen that statistically significant pollen counts could not be achieved. From l.u. 3 upwards pollen counts mostly of 300 total land pollen grains were achievable, and these show a succession characteristic of the onset of the Holocene in this region, from an *Empetrum*-dominated zone at the base (pollen zone KH2-a), through an interval in which *Empetrum* and *Juniperus* vary in their relative importance (KH2-b and

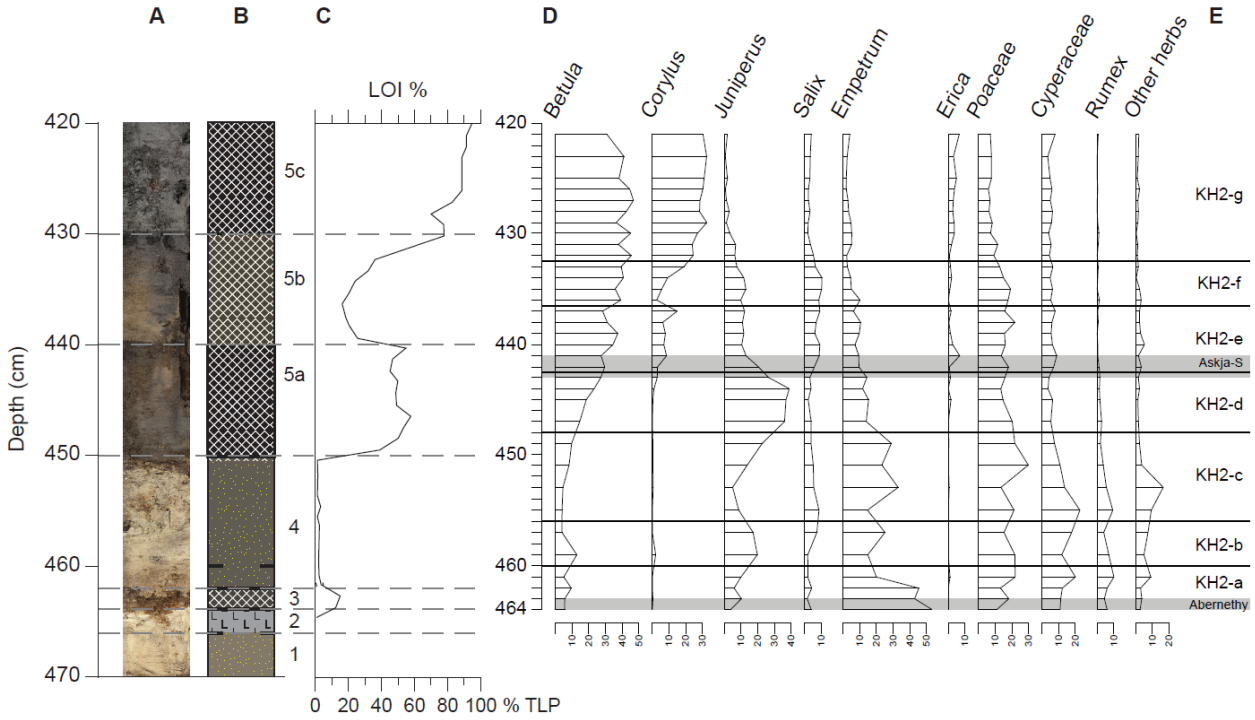


**Figure 5.** **A.** Photograph of basal core from Kingshouse 2. **B.** The main lithological units identified. **C.** Loss-on-ignition variations. **D.** Selected pollen taxa shown as variations in percentage of a pollen sum of total land pollen. **E.** Local pollen assemblage zones. The grey horizontal shading represents the intervals in which volcanic glass shards were detected, which are assigned to the Abernethy Tephra and the Askja-S Tephra (see text for details). . The lithological units represented are: 1. Silts and fine sand. 2. Clay-silts. 3. Moss layer. 4. Mainly silts, but some clay and fine sand inclusions. This unit contains isolated moss stems throughout. 5a. Organic mud. 5b. Organic mud with higher clay content. 5c. Organic mud with increased plant macrofossil content.

KH2-c), above which a clear *Juniperus* peak is evident (KH2-d), in turn succeeded upwards by notable increases in *Betula* and *Corylus* pollen (KH2-e to KH2-g). This sequence bears resemblance to that reported from the site by Walker and Lowe (1977), except in the following respects. First, much more detailed information is available for the lowermost pollen zones KH-2a to KH2-c, probably as a result of the use of improved pollen recovery methods, and this reveals a significant oscillation in *Juniperus* pollen, the reduced values of which (in zone KH2-c) are coincident with increased representation of Poaceae, *Rumex* and other herbaceous taxa. Second, an oscillation in *Corylus* pollen is also evident (zone KH2-f)

which falls within a distinct drop in LOI values (l.u. 5b). This *Corylus* drop is also represented in the same approximate position in the diagram published by Walker and Lowe (1977) where it is less well resolved, while no LOI data were included in that study. Whether these features represent purely local (site-specific) or wider influences (e.g. climate forcing) is difficult to judge and is not considered here.

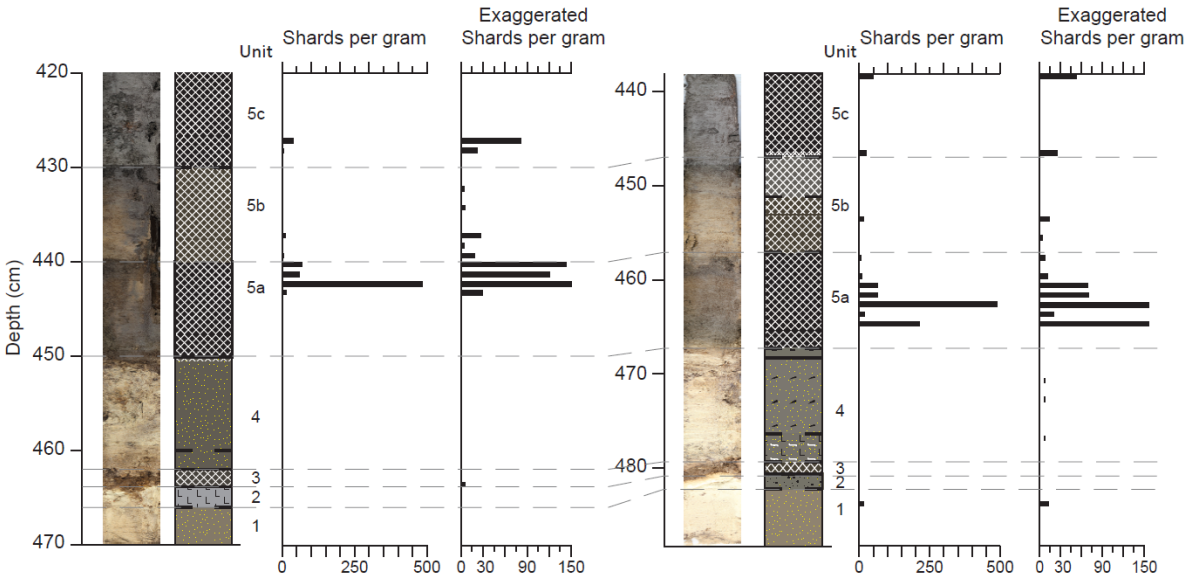


**Figure 6.** Distribution of non-visible glass shards (cryptotephra) through cores 2 (left side) and 3 obtained from the Kingshouse 2 site in 2015, measured in numbers of shards per gram of sediment. The exaggerated data do not show in full those values in excess of 150 shards per gram.

Traces of non-visible volcanic glass shards (cryptotephra) were detected in discrete intervals through two of the 2015 cores (**Figure 6**) using the procedures described in **Appendix B.4**. Consistent lithostratigraphic units and boundaries provide a means of cross-comparison between the two cores, where differences can be seen in the positioning and abundance of shards recorded in equivalent lithological units. These in part may reflect localised variations in the rate of sediment accumulation within the units. The most consistent and best developed tephra layer occurs within l.u.5a, the geochemical results for

which, and the laboratory procedures adopted, are provided in **Appendices C, D** and **B.4**. A total alkali versus silica (TAS) plot (**Figure 7A**) indicates these glass shards to be rhyolitic in composition and when compared with documented tephras from N. Europe dating to between 16 and 8 ka (Timms et al., 2019), to align closely with the distinctive Askja-S Tephra. Bi-plots of major oxides, most notably of CaO-FeO (**Figure 7B**) and $K_2O$-$TiO_2$ (**7C**), support this affiliation. This tephra has been detected in deposits dating to the very early Holocene in Iceland (Sigvaldason, 2002), Sweden (Davies et al., 2003; Lilja et al., 2013), Norway (Pilcher et al., 2005), Ireland (Turney et al., 2006), the Faroe Islands (Lind and Wastegård, 2011), Germany (Lane et al., 2012), Switzerland (Lane et al., 2011), the Orkney Islands (Timms et al., 2017, 2018), Wales (Jones et al., 2017), Romania (Kearney et al., 2018) and two sites in Scotland in the Glen Roy-Glen Spean catchment, named Inverlair and Turret Bank (Kelly et al., 2017; Lowe et al., 2017). The stratigraphical data reported here are consistent with the published data from Inverlair and Turret Bank, in that the tephra assigned to the Askja-S in all three sites is associated with the upper part of the early Holocene *Juniperus* phase (**Figure 5**).

Small traces (~11 shards $g^{-1}$) of volcanic glass were also recovered from the minerogenic sediments near the base of the sequence, at the base of the moss band (l.u.3; **Figure 6**). EPMA (electron-probe microanalysis) characterisation of this layer yielded 8 chemical analyses which demonstrate the rhyolitic nature of the shards. The data can be separated into two distinct groups according to differing compositions of a number of elements (**Figure 7**), in particular FeO and CaO (wt%). Recent detailed tephrostratigraphic studies in Scotland (e.g. MacLeod et al., 2015; Timms, 2016; Timms et al., 2017, 2018) provide useful comparatives to this layer identified at Kingshouse. The first chemical group matches closely the rhyolitic chemistry of the Katla volcano (Iceland), and the tephra's stratigraphic position, in relation to the associated radiocarbon dates and lithostratigraphic

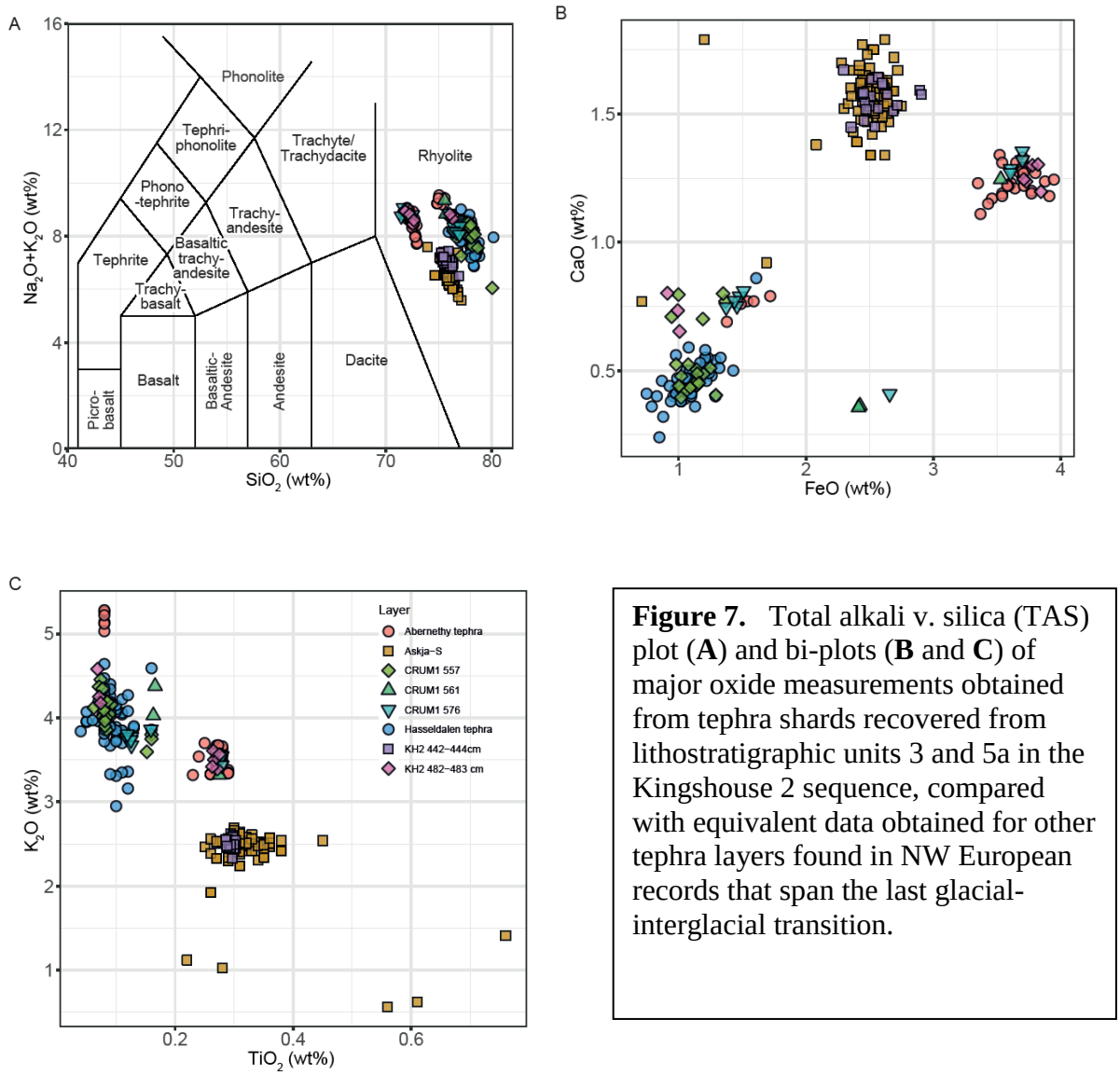


**Figure 7.** Total alkali v. silica (TAS) plot (**A**) and bi-plots (**B** and **C**) of major oxide measurements obtained from tephra shards recovered from lithostratigraphic units 3 and 5a in the Kingshouse 2 sequence, compared with equivalent data obtained for other tephra layers found in NW European records that span the last glacial-interglacial transition.

data, has led us to assign it to the Abernethy Tephra (MacLeod et al., 2015). The second chemical group comprises three analyses with lower FeO and CaO values than group one. These data are similar to those of tephras identified as having a 'Borrobol-type' chemistry. This chemical signature is found intermittently within the last glacial-interglacial transition (the interval between ~16 and 8 ka BP), including early Holocene deposits in Scotland. In particular it is found at Crudale Meadow (Orkney) in association with rhyolitic shards from Katla (Timms et al., 2018), but, significantly, also with shards correlated with the

Hässeldalen Tephra, which is broadly contemporaneous with the Abernethy Tephra (Bronk Ramsey et al. 2015).

### 4.2 *Radiocarbon chronology*

Several of the basal cores were sieved for plant macrofossil remains (see **Appendix B.5**) to provide material for radiocarbon dating, but only the samples obtained from the core depths listed in **Table 1** provided sufficient material for analysis by accelerator mass spectrometry (AMS). The initial aim was to submit samples to the radiocarbon laboratory consisting purely of terrestrial vascular plant remains, excluding moss species, but this proved possible for only a few samples. The most abundant fossil remains encountered were derived from mosses, mainly *Racomitrium aciculare* (yellow fringe moss), *R. lanuginosum*, *Pogonatum* spp. (spike moss or 'haircaps') and *Scorpidium scorpioides* (hooked scorpion moss). Some of the dated samples consisted of a mixture of moss and angiosperm terrestrial plant material, while two dates are based purely on moss material, for comparison purposes. The angiosperm plant remains were mainly derived from *Betula nana* (dwarf birch), *Carex* spp. (sedge) and ericoid species (*Empetrum nigrum* and *Vaccinium* spp.), and included seeds, budscales, leaf fragments and occasional woody fragments. Remains of obligate aquatic taxa (e.g. *Potamogeton* seeds) were removed from the samples. Radiocarbon activity of the samples was determined at the Oxford Radiocarbon Accelerator Unit (ORAU), Oxford University, UK, using the pretreatment and analytical procedures outlined in **Appendix B.5**. The amount of carbon available for AMS analysis, was generally low (**Table 1**) due to the exclusion of material derived from aquatic plants, a major component of the macrofossil content of the basal sediments. However, all the dated samples were large enough to be measured using routine AMS wheels at Oxford, the analytical error ranges obtained are of standard precision, and the age estimates are in chronological order by sample depth, within the 95% errors. Note, however, that dates from samples consisting solely of, or including,

| Depths (cm) in cores 3 and 4 | Depths (cm) in core 2 | Stratigraphic feature | weight carbon (mg) stage 1 | weight carbon (mg) stage 2 | dated material | radiocarbon date (BP) | $\delta^{13}C$ (‰) | laboratory reference no. | 2 sigma cal. a BP range |
|---|---|---|---|---|---|---|---|---|---|
| 452-450 | 432-430 | top of litho-unit 5 | 3.61 | 1.97 | *Betula* sp. Seeds & twigs | 9146 ± 39 | -27.20 | OxA-35596 | 10419-10229 |
| 460-459 | 443.5-442.5 | *ASKJA-S TEPHRA* | - | - | - | - | - | - | - |
| 467-466 | 451-450 | litho-unit 4/5 transition | 15.14 | 1.67 | Leaf fragments- *Vaccinium* sp. and undiff.; *Polytrichum* cf. *commune* & *Racomitrium* sp. | 9935 ± 45 | -23.27 | OxA-32469 | 11386-11208 |
| 478-476 | 462-460 | lower litho-unit 4 | 2.36 | 1.18 | Leaf fragments and seeds, *Empetrum nigrum* & undiff. | 9825 ± 45 | -29.70 | OxA-35411 | 11315-11183 |
| 478-476 | 462-460 | lower litho-unit 4 | 3.85 | 0.78 | *Polytrichum* cf. *commune* & *Racomitrium* sp. | 9920 ± 60 | -22.73 | OxA-35410 | 11508-11218 |
| 479-478 | 463-462 | litho-unit 3 | 4.16 | 1.90 | Leaf fragments - *Betula nana*, *Vaccinium* sp., *Dryas* sp., *Salix herbacea* & undiff. | 9870 ± 40 | -28.61 | OxA-32470 | 11604-11239 |
| 480-478 | 464-462 | litho-unit 3 | 4.29 | 0.92 | Leaf fragments- *Vaccinium* sp., *Empetrum nigrum* & undiff.; twigs undiff. | 9860 ± 50 | -29.18 | OxA-35409 | 11368-11198 |
| 480-478 | 464-462 | litho-unit 3 | 16.25 | 1.94 | *Racomitrium* sp. | 9915 ± 45 | -24.13 | OxA-35408 | 11411-11224 |
| 480-479 | 464-463 | *ABERNETHY TEPHRA* | - | - | - | - | - | - | - |
| 485-484 | 467-466 | upper litho-unit 1 | 10.99 | 1.58 | Leaf fragments- *Vaccinium* sp., *Betula nana*; *Racomitrium* sp. & *Polytrichum* cf. *commune* | 10015 ± 45 | -23.22 | OxA-32471 | 11747-11292 |

moss remains could be subject to inbuilt age errors. Where dates based on moss can be compared directly with dates based on terrestrial angiosperm material obtained from the same stratigraphic horizons (cf. samples OxA-35410 and OxA-35411, **Table 1**), the moss age estimates are older by up to ~100 $^{14}$C years. This inbuilt age problem may also extend to samples that are partially based on moss material, for sample OxA-32469 registers an enriched $\delta^{13}$C value compared with those based wholly on terrestrial angiosperm remains, and has an estimated age error of ~360 years (see section 5.2). This probably reflects the uptake by some moss species of dissolved inorganic carbon, which dilutes the $^{14}$C activity ratio leading to an 'apparent age' factor, a problem encountered in other studies where moss remains were used (e.g. MacDonald et al. 1987; Sveinsbjörndóttir et al., 1992). This particular problem is more commonly encountered, and indeed is more pronounced, in radiocarbon dates obtained from the remains of aquatic plants (Marty and Myrbo, 2014), the reason we excluded such material in the present study.

The presence of two cryptotephra layers in the Kingshouse 2 basal sequence provides a means of testing the reliability of the radiocarbon chronology, since they have been dated independently in other studies. The most robustly dated is the Askja-S Tephra, the mean age of which, based on combining radiocarbon chronologies obtained from several European sites, is 10.82 ± 97 cal $^{14}$C ka BP with a 2σ error range (Kearney et al. 2018), an estimate that accords well with the Kingshouse 2 radiocarbon data (**Table 1**). An older date of 11.23 ± 226 cal $^{14}$C ka BP has been suggested for this tephra based on evidence from a site in Poland (Ott et al. 2016), but this is an outlier compared with the majority of dates available (Kearney et al. 2018). For completeness, however, both age estimates are employed in separate age models presented in **Appendix F**.

The older tephra in the Kingshouse 2 sequence, assigned to the Abernethy Tephra (AT), is more equivocal, because of its close chemical similarity with the Vedde Ash (VA), which dates to ~12.1 ka BP (Bronk Ramsey et al., 2015): it has been argued that small traces of glass shards that have been assigned to the AT could be reworked VA instead (see Timms et al., 2019). This is unlikely in this case, however, because the VA is usually the most prominent peak in glass shard concentrations in Lateglacial deposits in sites in the Scottish Highlands, and if present in the Kingshouse 2 basin, it should be more strongly represented. The facts that these trace amounts of Katla type tephra are (i) found near the Stadial-Holocene transition, which is consistent with other tephra layers assigned to the AT (MacLeod et al., 2015) and (ii) are associated with shards of Hässeldalen Tephra (see section 4.1), makes it more likely that it represents an early Holocene ashfall event. Furthermore, although the reported age range of the AT of 11.46 ± 122 $^{14}$C cal ka BP is not well constrained, being based on the radiocarbon evidence obtained from a single site (Matthews et al., 2011; Bronk Ramsey et al. 2015), it is compatible with the independently-derived radiocarbon chronology (**Table 1**). Hence, while regarded as provisional until more secure data become available, it has been adopted in the construction of the age models presented in the following section.

### 4.3 *Age models*

Age models based on the radiocarbon and tephrochronological data outlined above were constructed using the Bayesian statistical program OxCal version 4.3 (Bronk Ramsey, 2017) and the IntCal13 calibration curve (Reimer et al., 2013). Model outputs were computed using a 'P_Sequence' deposition model (Bronk Ramsey, 2009a) with a variable k parameter enabling the program to determine optimal age-depth relationships (Bronk Ramsey and Lee, 2013). A 'general' outlier model was applied in OxCal such that each of the radiocarbon dates was given an *a priori* 5% probability of being a statistical outlier (Bronk

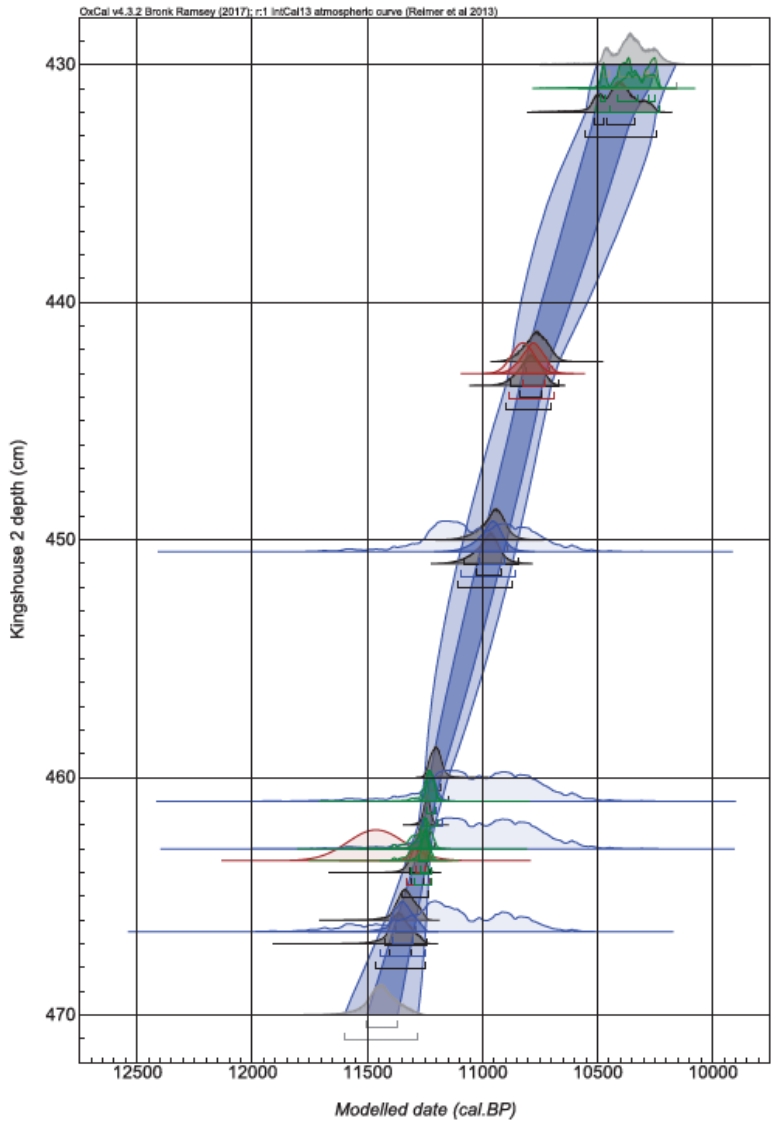


**Figure 8.** Bayesian 'P_Sequence' age-depth model for the Kingshouse 2 basal sediment sequence produced using OxCal version 4.3 (Bronk Ramsey and Lee, 2013) and the IntCal13 calibration curve (Reimer et al., 2013), and incorporating the age estimate for the Askja-S Tephra of Kearney et al. (2018). Light blue and dark blue shading show the limits of the 95.4% and 68.2% probability ranges respectively.

Ramsey, 2009b). The age model coding sequence is provided in **Appendix E**. Three age models were constructed (**Appendix F**), an initial model scenario using the radiocarbon dates alone, and two scenarios that combined the radiocarbon and tephrostratigraphic age estimates, one employing the Ott et al. (2016) and the other the Kearney et al. (2018) age ranges for the Askja-S Tephra. All three scenarios show very similar age-depth plots that

imply near-linear sedimentation rates through the depth interval analysed, while there is minimal difference between them in terms of the 95.4% probability ranges they compute for the age of the base of the Kingshouse 2 sequence. The preferred option (**Figure 8**) is that which employs the Kearney et al. (2018) Askja-S age estimate, for the reason given in section 4.2, which is also the most precise model. Adopting this best-estimate age model provides the time axis employed in **Figure 9** and a robust chronology for changes in the local vegetation cover. Fuller details of the vegetation succession represented in **Figures 5** and **9** will be considered elsewhere; here we focus only on points relevant to the timing of the deglaciation of Rannoch Moor. The data suggest that the earliest datable sediment in the Kingshouse 2 basin began to accumulate ~11,500 years ago, while the first countable pollen horizons date to ~11,300 years ago, and for about 300 years afterwards the local catchment appears to have remained treeless, with a predominantly open landscape colonised by juniper (*Juniperus*) and crowberry (*Empetrum*), while open water supporting an aquatic flora dominated by *Potamogeton* (pondweed) flourished in the basin (zones KH2-a to KH2-c, **Figure 9**).

## 5. Discussion

### *5.1 When did the SW Highland icefield begin to recede?*

The new evidence we have presented above, which suggests that LLR ice in the vicinity of the western part of Rannoch Moor did not decay until at the earliest ~11,500 years ago, is in accord with four other age estimates that constrain the timing of the demise of the SW Highland icefield. First, it is remarkably in line with the estimate of 11.5 ± 0.6 ka derived by Small and Fabel (2016a) from $^{10}Be/^{9}Be$ ratio measurements obtained from the surfaces of

granite boulder erratics deposited by LLR ice in the same vicinity (section 4). Second, near the margin of the major LLR ice lobe in the Loch Lomond area (**Figures 1, 2**), a series of

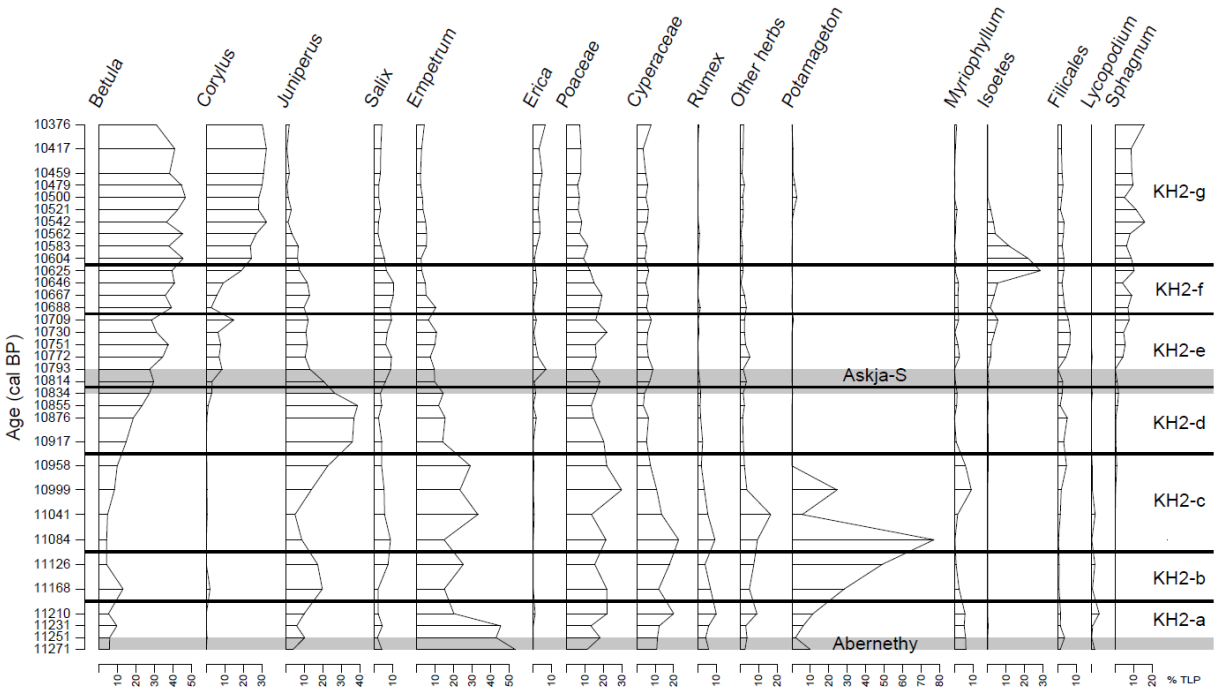


**Figure 9.** Percentage pollen data (% total land pollen) for selected taxa and the positions of the Askja-S and Abernethy tephras for the Kingshouse 2 sequence shown on a time axis using the Bayesian-based age model presented in Figure 8 and discussed in the text. The local pollen assemblages zones (final column) as in Figure 5.

radiocarbon dates obtained from organic debris buried by the advancing glacier margin, coupled with analysis of varved sediments that accumulated in a lake (Glacial Lake Blane) dammed by the advancing ice, indicates that the Loch Lomond glacier was still advancing after 12.0 cal $^{14}$C ka BP and did not start to recede until ~11.74 cal $^{14}$C ka BP or later (MacLeod et al., 2011). Third, in the Glen Spean and Glen Roy area (**Figures 1, 2**), detailed analysis of varves that accumulated in lakes dammed by advancing ice fronts (the Roy-Spean ice-dammed lakes), coupled with tephrostratigraphical studies, also indicates that glacier lobes in this area were still advancing after ~12.1 ka BP and appear to have persisted as

competent barriers that held back major ice-dammed lakes until ~11.6 ka BP (Palmer et al., 2010, 2012; Palmer and Lowe, 2017). Fourth, analysis and dating of glacimarine deposits in the Muck Deep (**Figure 1**), a glacially over-deepened trough in the Sea of the Hebrides off the west coast of Scotland, indicates local glaciation continued until ~11.9 ka BP (Arioso and Howe, 2018). All of these records are therefore consistent in suggesting that LLR ice, at least in these localities, did not start to recede until towards the end of the GS-1 interval, and may have persisted in some places after the onset of the Holocene.

It is pertinent to reflect on the palaeo-glaciological context of the three studies on the Scottish mainland referred to above, which have been dated independently. The Loch Lomond lobe was fed by ice draining southwards from a very large catchment enclosing much of the southern part of the SW Highland icefield (**Figure 2**), while the limits in Glen Spean and Glen Roy were fed mainly by ice advancing from the west, from the Nevis and adjacent mountain ranges, but with a contribution from the Treig Glacier, sourced from the Rannoch basin. The evidence summarised above therefore indicates that the northern and southern extremities of the SW Highland icefield, as well as the main ice shed over the Rannoch basin, were responding quasi-synchronously to the same forcing factor(s). The alternative possibility that the chronologies we have presented are seriously flawed in all four cases seems unlikely, especially since they are collectively based on four different dating methods. A final point to note is that these data imply LLR ice retreated from the lowland terminal lobes in Loch Lomond and Glen Roy shortly before ice shrank from the ice shed over the Rannoch basin, which seems logical. The conclusion reached by Bromley et al. (2014, 2018), however, for ice seemingly disappearing from the Rannoch ice shed by 12,200 or even possibly by 12,500 years ago, is difficult to reconcile with the scenario we have presented. To illustrate the point, the radiocarbon measurements that they base their

conclusions on are plotted against those synthesised above in **Figure 10**. In the following section we consider possible reasons for this significant discrepancy.

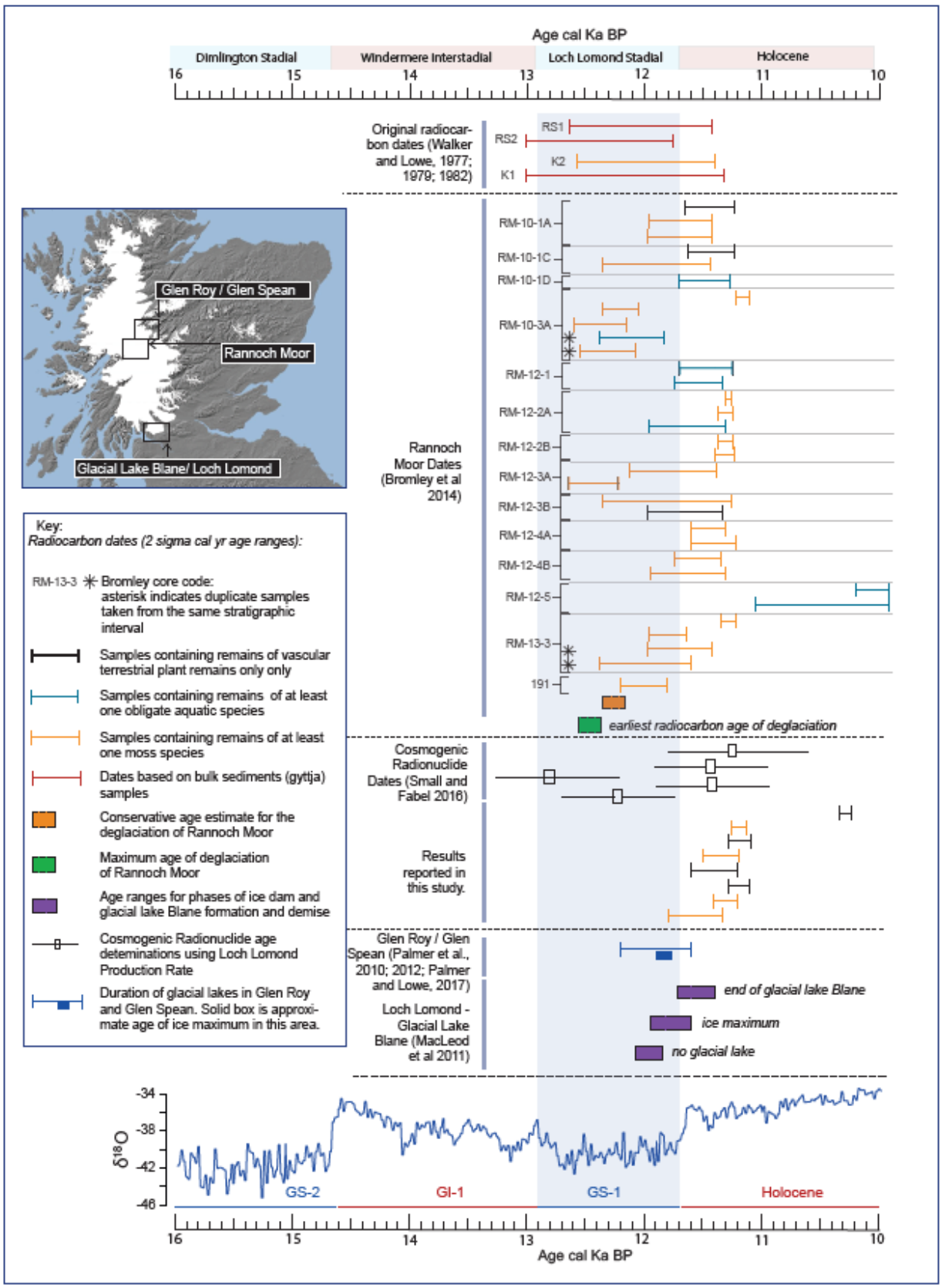


**Figure 10**. Plot of all radiocarbon (2-sigma), cosmogenic radionuclide (1-sigma) and other age estimates referred to in this contribution, shown against the Greenland stratotype sequence for the period 16 to 10 cal ka BP. For further explanation see text.

5.2 *Critique of the Rannoch Moor radiocarbon data-set presented by Bromley et al.*

Bromley et al. (2014) presented the results of 32 radiocarbon measurements obtained from 13 basal sediment cores recovered from 8 kettle basins located between LLR recessional moraine ridges on Rannoch Moor. Their dataset is reproduced here in condensed form in **Appendix G**, with individual 2 sigma age ranges plotted in **Figure 10.** It was on the basis of these data that Bromley et al. concluded that some basins became ice-free by possibly as early as ~12.5 cal $^{14}$C ka BP, a view reinforced in Bromley et al. (2018). However, we consider the chronological basis for this conclusion to be highly tenuous, for the following reasons. The first thing to note is that very little stratigraphical context is provided for the samples from which their dates were obtained. Generalised and subjective basal lithostratigraphic descriptions are provided in Bromley et al.'s (2014) *Supplementary Information*, but these vary in the nature and succession of stratigraphic units indicated, while no quantified measures (e.g. loss-on-ignition), biostratigraphic or other data are provided to help establish independent correlations between the cores. Hence, while there is superposition control for samples obtained from within an individual core, this control is lacking when attempting to compare results between different basins. It is also difficult to assess whether the basal sediments accumulated conformably or were subject to reworking or other complications, in the absence of supporting stratigraphic or proxy environmental details.

A second observation is that out of the 32 calibrated dates on which their conclusions rest, only five provide weighted means older than 12.0 cal $^{14}$C ka BP, and of these 5, four are from the basal deposits of core RM-10-3A (**Appendix G**). Hence, in only 2 of the 8 basins do they obtain data that might support their proposal. The mean of all 32 calibrated radiocarbon results is ~11.57 cal $^{14}$C ka BP, and if the five dates greater than 12.0 cal $^{14}$C ka BP are excluded (for reasons given below), the overall mean for the reduced data-set is ~11.43 cal $^{14}$C ka BP, a value close to that suggested by our age models for the onset of

sedimentation in the Kingshouse 2 basin (section 4.3). A further significant observation concerns the only records obtained by Bromley et al. (2014) that we can directly compare with, which are those listed as having been recovered from the Kingshouse 2 basin: these are the data reported from cores RM-12-2A, RM-12-2B and RM-13-3 (**Figure 10** and **Appendix G**). The oldest basal dates they obtained from each of these cores are 11.58 ± 158, 11.33 ± 52 and 11.99 ± 191 cal $^{14}$C ka BP, with a mean of ~11.6 cal $^{14}$C ka BP. Again, these data are consistent with our proposed timing for the onset of the retreat of LLR glaciers on and adjacent to Rannoch Moor, though it is difficult to assess the robustness of these statistical comparisons in the absence of common stratigraphical tie-lines between the records.

With respect to the five radiocarbon measurements listed in **Appendix G** with age estimates >12.0 cal $^{14}$C ka BP, the following reservations should also be considered. Four of the five samples contain remains of moss (*Pogonatum*), and the fifth includes remains of the aquatic algal charophytes *Chara* and *Nitella*. The possibility that these components could introduce artificial ageing errors was alluded to in section 4.2, where we have presented evidence that suggests that samples containing moss can give older dates than contemporaneous terrestrial angiosperm plant remains. One way of assessing possible aberrance of radiocarbon age measurements is through analysis of the $\delta^{13}$C content of the measured samples, but those data are not supplied by Bromley et al. (2014). The data we have presented from Kingshouse 2 (**Table 1**) clearly show that $\delta^{13}$C‰ values obtained from samples containing moss remains diverge from average values expected from terrestrial land plants (see Bowman, 1990; Boutton, 1991), something also noted by Lowe and Walker (1976) with respect to their original radiocarbon measurements obtained from this sequence. Furthermore, Bromley et al. (2014, p. 6219) discount this possible source of error when stating that "… contamination by dissolved old carbon (the hard-water effect) is unlikely to affect our samples due to *the absence of carbonate lithologies* in the surrounding area and our

preferential selection of terrestrial species for radiocarbon analyses." Lowe and Walker (1979) also assumed this to be the case, but this claim may be false because some geological surveys of the area have indeed recorded bands of crystalline limestone, marble and calcite-cemented breccias amongst the rocks underlying Rannoch Moor (Hinxman et al., 1923; Smith and Marsden, 1977), although their areal extent is difficult to gauge since most of the rock surface is obscured by thick peat. An alternative and possibly more likely source of calciferous material might be the glacial deposits that enclose the kettle depressions, derived from source rocks that border the Rannoch basin. In this respect, a particular difficulty we encountered when preparing samples for radiocarbon measurement was the complete removal of particles trapped between leaves and fronds (**Figure 11**). Tiny sediment particles containing inert carbon could possibly have survived the vigorous cleansing procedures applied during sample pretreatment (**Appendix B.5**) in the innermost recesses of subfossil remains. In combination, these uncertainties compromise the approach adopted by Bromley et al. (2014, p. 6216), which was to "…take the single oldest age in our dataset as the closest constraint on deglaciation." The problem with basing interpretations entirely on dating results that are unconstrained stratigraphically is that their credibility cannot be properly interrogated, while the oldest dates could simply be statistical outliers.

The potential offset of dates obtained from samples that included moss remains, which may provide an index of the scale of inbuilt reservoir errors, can be computed from our age models; the results (**Figure 12**) suggest that one moss sample has a potential reservoir error of 361±54 radiocarbon years (95.4% CI), with others having reservoirs of between 79-108 radiocarbon years (mean estimates). This suggests that the carbon reservoir varied during the early Holocene, most likely reflecting variations in catchment stability, water levels, substrate type, percentage of moss in the sample, and/or moss species sampled. It might seem counterintuitive to suspect that moss species from the Polytrichaceae family would be

**Figure 11.** Small sediment particles adhering to subfossil shoots of a species of the moss genus *Racomitrium* (probably *R. lanuginosum*). The coarser particles were removed by immersion in, and jet-spraying by, deionised water. Very fine particles were removed by radiocarbon pretreatment procedures described in **Appendix B.5**.

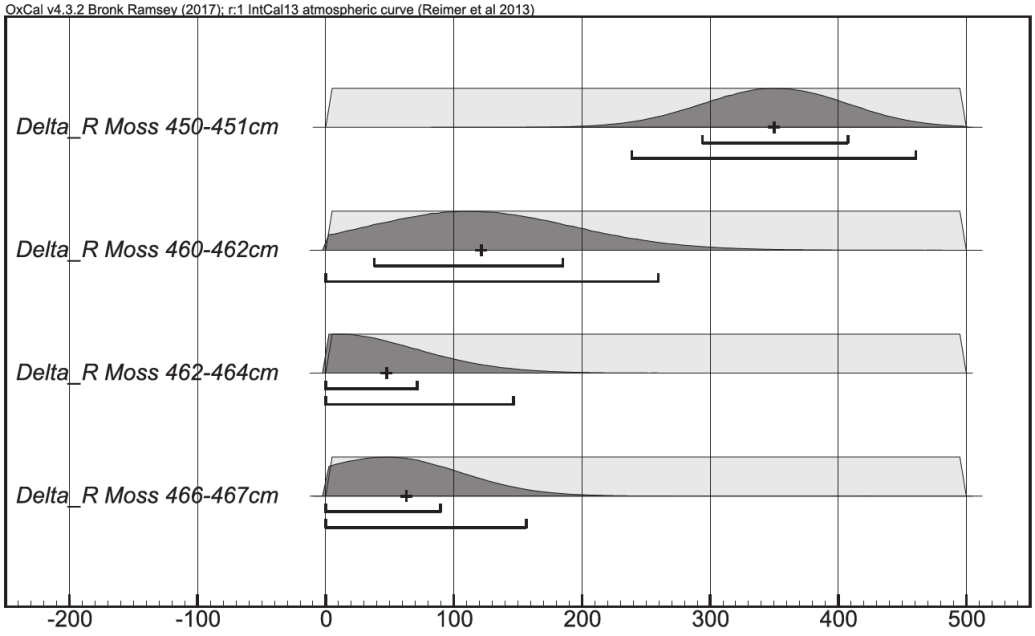


**Figure 12**. Potential reservoir effect (Delta R) of samples containing moss remains, derived from the age model constructions presented in **Appendix F**.

influenced by a reservoir from an aquatic source as they are often considered to occupy dry disturbed soils in upland moorland conditions. However, species like *P. commune* are known to occupy wet moorland and bog, to tolerate waterlogged anoxic conditions (Watson, 1981),

and even to have growth forms within open pools of water fed by snow melt (Sarafis, 1971). The other mosses identified in the Kingshouse sequence include species of *Sphagnum* and *Racomitrium*, known to occupy a range of conditions from relatively dry moorland to wet and waterlogged conditions (Watson, 1981), which may also acquire carbon from an aquatic source. Whatever the reason/s for this offset, it indicates that dates from mosses, and by inference aquatic material, may be considered subject to 'ageing' effects making them appear older than their 'true age', though this will only apply to a subset of the dates acquired which could be assessed using enriched $\delta^{13}C$ values as an indicator. The Bromley et al. (2014) dataset cannot be appraised in this way, however, and hence dates based on samples containing moss and aquatic remains should have additional caveats placed on their interpretation.

Of course, some of the problems summarised above could also afflict the dates that we have presented, and indeed we have highlighted where there is some evidence for possible bias. Nevertheless, several convergent lines of evidence support our general view that the earliest deposits to accumulate in the Kingshouse 2 basin, and indeed in other basins on Rannoch Moor, did so at the start of the Holocene: (i) the earliest polleniferous sediments show a succession typical of the onset of the Holocene (**Figure 5**); (ii) two tephra layers provide independent corroboration of this; and (iii) the greater reliance placed on radiocarbon dates based on terrestrial plant remains with moss remains excluded (**Table 1**). We concede, however, that the lowermost sediments in the Kingshouse 2 sequence are non-polleniferous, and thus lack definitive evidence of their age (**Figure 5**), while we acknowledge the point made by Bromley et al. (2014), but which has long been appreciated (e.g. Böse, 1995; Ham & Attig, 1996; Henriksen *et al*. 2003), that glacier ice could have survived in kettle holes for some time after surrounding ice had melted. Nevertheless, we contend that the most likely scenario for the development of the basal sediment sequence in the Kingshouse 2 basin is as

follows: (1) a pond developed within the basin very soon after deglaciation, and because surrounding slopes were unvegetated and unstable, sands and silts accumulated rapidly in the base of the hollow either through slope wash or collapse of the basin margins (litho-unit 1, **Figure 5**); (2) this process was temporarily interrupted, allowing clays and silt to accumulate and mosses to colonise the basin margins (litho-units 2 and 3); (3) further degradation of the slopes took place but during a time when aquatic plants colonised the pond (see **Figures 5** and **9**) and land plants progressively colonised adjacent slopes (litho-unit 4); (4) higher plants continued to invade the area, allowing soils to develop and the basin margins to stabilise (litho-unit 5). There is no compelling evidence to suggest that events were more complex or protracted.

It should be noted that the chronological evidence we have presented from the Kingshouse 2 site provides an age estimate for the melting of LLR ice in the vicinity of the former ice shed that occupied the western part of the Rannoch basin (Fig 2), and not for when the LLR icefield began to shrink. Geomorphological maps of the crests of LLR moraines in the western part of the Rannoch basin clearly indicate progressive recession of the icefield's margin across this area in an approximately NE to SW direction (Bickerdike et al., 2016; Hornsey, 2016), which is the opposite to the trend suggested by Bromley et al. (2014, p. 6216, in caption for Fig. 2). The question that arises, therefore, is when did this sequential retreat commence? A review of the currently available stratigraphical evidence from the Glen Spean and Glen Roy valleys suggests that the northern margins of the LLR icefield did not start to recede until ~11.6 ka BP (Palmer and Lowe, 2017). If that interpretation is correct, then it suggests very rapid retreat of the ice, if it was to reach and expose the Rannoch basin just 100 years later. Perhaps the ice in the lower valleys down-wasted catastrophically, which would fit with the evidence for extensive suites of fluvioglacial

landforms mapped throughout the Spean Valley by Sissons (1979a, 1979b, 2017). Ice retreat across the Rannoch basin appears to have been more controlled by comparison.

### 5.3 *The wider picture*

The long-held concept of a regionally synchronous 'Younger Dryas' event that consigned NW Europe to persistently severe climatic conditions for 1200 years or more is increasingly being questioned. Lake basin records from this region, when examined at a sufficiently high temporal and stratigraphic resolution, are revealing that the interval between ~12.9 and 11.7 ka BP was probably two-phased, with a significant shift in prevailing climatic conditions in the middle of the interval (Bakke et al. 2009; Neugeberger et al., 2012; Lane et al., 2013). A two-phased pattern for this period has also been detected in a number of speleothem records from the Iberian peninsula, the timing of the phase change generally dating to between ~12.5 and ~12.15 ka BP (Baldini et al., 2015; Bartolomé et al., 2015; Rossi et al., 2018). This regional change appears to reflect migration of the North Atlantic Polar Front (NAPF), long considered a major factor determining the prevailing climatic conditions in Europe during the late Quaternary (e.g. Ruddiman and McIntyre, 1976, 1981; Mix and Fairbanks, 1985), and reinforced in more recent studies (e.g. Eynaud et al., 2009). Southward migration of the NAPF in the eastern North Atlantic leads to southward displacement of the westerly storm tracks that are a dominant feature of the modern climatic régime in the NE Atlantic area. The lake and speleothem studies referred to above indicate that prior to ~12.5 ka BP the NAPF and the westerly storm tracks were positioned south of the Iberian peninsula (Baldini et al., 2015; Bartolomé et al., 2015), after which the NAPF re-migrated northwards reaching Norway after 12.17 ka BP, bringing more variable, perhaps stormier, conditions to northwestern Europe (Bakke et al., 2009; Lane et al., 2013).

It seems highly likely that this shift in position of the NAPF would also have affected the Scottish Highlands, raising questions about the possible impacts this may have had on prevailing climatic conditions and contemporaneous glacial ice cover. Bromley et al. (2014) propose that the SW Highland icefield was at an advanced state of terminal decline possibly by ~12.5 cal $^{14}$C ka BP, and conservatively by 12.2 cal $^{14}$C ka BP, attributing this to the development of warmer summers in Scotland as a result of increased seasonality driven by stratification of the North Atlantic. We have argued, however, that this speculation is predicated on questionable chronological information, while expansion of the SW Highland icefield appears to have continued until at least the end of the GS-1 interval, with significant retreat delayed until after the start of the Holocene.

A late GS-1 readvance of ice is not only suggested for Scotland, for some glaciers in parts of western and south-western Norway also readvanced at this time (Bondevik and Mangerud, 2012; Mangerud et al., 2016) while rapid retreat of the ice sheet in western Norway and from the Ra Moraine in the Skagerrak area did not commence until ~11.6 ka (Mangerud et al., 2019; Romundset et al., 2019). Ice growth also continued after the onset of the Holocene in some parts of Svalbard (Farnsworth et al., 2018). Furthermore, independent palaeoclimatic studies based on a range of palaeobiological data indicate that cold conditions persisted in western Norway until ~11.5 cal $^{14}$C ka BP (Gulliksen et al., 1998), in Denmark tundra vegetation prevailed beyond the start of the Holocene (Bennike and Mortensen, 2018) and temperatures in SW Sweden remained cold until around 11.56 cal $^{14}$C ka BP, and were most severe during the later part of GS-1 (Wohlfarth et al., 2018). Therefore, evidence is increasingly pointing to cold conditions having prevailed throughout parts of NW Europe until or beyond the start of the Holocene, and the new evidence we have presented for the SW Scottish icefield fits this scenario.

On the other hand, other evidence points to a more complex glacial history during the GS-1 chronozone. For example, while the margins of the Scandinavian ice sheet readvanced in some areas during this interval, other margins remained stationary or continued with recession that had commenced during the preceding interstadial (Mangerud et al. 2016). In Scotland, cosmogenic nuclide dating of erratic boulders indicates that a number of independent LLR ice masses in the NW Highlands and on the Isles of Skye and Harris appear to have reached their maxima and started to retreat well before the end of GS-1 (Ballantyne, 2007, 2012), a conclusion also prompted by the results of numerical simulations of LLR glacial growth and decay in Scotland (Golledge et al., 2008). The picture that is emerging, therefore, is of significant diachronous behaviour of LLR glaciers during GS-1, even with respect to different glacier tongues radiating from the same relatively small mountain icefield (Lukas and Bradwell, 2010; Finlayson et al., 2011). One possibility is that this may reflect the size of the glacier body, with small ice masses being quicker to respond to external influences than larger icefields which displayed greater inertia. This speculation may prove simplistic, however, for other factors may prove to have been equally or more important in determining glacier behaviour during GS-1, a matter that is for future research to clarify.

## 6. Conclusions

The new evidence we have presented from the Kingshouse 2 site leads us to reject Bromley et al.'s (2014, 2018) proposal that the Rannoch Moor area was deglaciated as early as ~12.5 cal $^{14}$C ka BP. We find the radiocarbon dataset on which they base their proposals to be contestable because: (i) the dated samples are stratigraphically unconstrained; (ii) no $\delta^{13}$C data are provided, so that the possible influence of hard-water (ageing) errors cannot be assessed; and (iii) they accentuate the importance of the oldest age estimates they obtained, which is statistically questionable. With respect to the third of these criticisms, the oldest dates were obtained from only two of the 13 sediment cores that they dated, and could merely

represent statistical outliers, but the limited stratigraphical context they have provided renders this difficult to test. We contend that the new evidence we have provided, which indicates that the Rannoch basin did not become ice-free until after the onset of the Holocene, is more secure because it is based on: (i) radiocarbon dates that are stratigraphically anchored; (ii) accordance between radiocarbon dates and independently-determined age estimates based on tephrochronology; and (iii) coherence with age estimates for the maximum expanse and subsequent recession of ice in two of the major outlets of the SW Highlands icefield, the Loch Lomond and Spean-Roy catchments. Our results are also consistent with age estimates for the deglaciation of Rannoch Moor based independently on surface exposure dating (Small and Fabel, 2016a), with evidence for glacimarine sedimentation persisting in the Sea of Hebrides until ~11.9 ka BP (Arosio and Howe, 2018) and with some climatic reconstructions for the later part of the GS-1 interval from neighbouring parts of NW Europe.

It therefore follows that we also reject two crucial implications that are predicated on the validity of Bromley et al.'s Rannoch Moor radiocarbon dataset. The first is the palaeoclimatic implication that deglaciation in Scotland in the middle of GS-1was driven by warming summers; no regional palaeoclimatic data were provided to support this assertion, so the supposition is based entirely on unconstrained radiocarbon dates, while quantified temperature estimates based on chironomid assemblages suggest that summer temperatures remained depressed during the later part of the GS-1 interval in the western Scottish Highlands (Brooks et al., 2016). Given that the Rannoch basin was the site of a major ice-dispersal centre feeding the SW Highlands icefield during the LLR, and the strength of the evidence we have presented for much later wastage of the ice, we view Bromley et al.'s proposal as glaciologically implausible. The second is the use of their radiocarbon data-set data to calibrate the $^{10}$Be isotope production rate for Scotland which, it is claimed, will yield

accurate $^{10}$Be surface-exposure ages in the British Isles (Putnam et al., 2019). We would counsel that this proposal may be predicated on false premises.

We acknowledge, however, that all age models have uncertainties, including those presented here, and that the need to analyse late Quaternary stratigraphical records with a sub-centennial resolution means operating at perhaps the technical limits of some dating methods. It is also the case that the total number of secure radiometric dates currently available for dating the LLR glaciation, and deglaciation, of Scotland is still very low considering the number and areal coverage of LLR glacier margins inferred from field evidence. There is therefore a need to develop a much more comprehensive chronological database, preferably one that enables cross-checking of dates obtained using two or more independent methods, and which includes data specifically designed to test hypotheses concerning spatial differences in the timing of LLR ice advance and decay, and their possible causal mechanisms.

Finally, and in the wider context, we have used this regional example to highlight the problems that can arise when terms such as 'Younger Dryas' are employed universally and in an unqualified manner. It is important to recognise and articulate the crucial differences in meaning between the chronostratigraphic, climatostratigraphic, or other use of this term - for example when referring to an event, such as an episode of glacier retreat or advance. There is a need to distinguish between the timing and nature of climatic shifts on the one hand, and of environmental responses to those shifts on the other hand. This requirement becomes more acute where past environmental changes can be reconstructed at a sub-centennial temporal resolution, and regional diachronous behaviour becomes apparent. Achieving these goals will require more comprehensive and secure interpretations of local stratigraphic information, and

a more forensic approach to the dating of key events than has generally been the case hitherto.

**Acknowledgements**

JL gratefully acknowledges financial support from *The Leverhulme Trust* (Emeritus Fellowship project EM-2014-025) which facilitated the field investigations and the procurement of the radiocarbon measurements reported herein, and the granting of access to the Kingshouse site by Mr. Graeme Ferguson of Bidwell's, Fort William, and by *Scottish Natural Heritage* (South Highland Fort William office). The authors thank Ben Chandler for permission to use his map of the Loch Lomond Readvance ice limits (Figure 1 herein), Jo Hornsey and the British Geological Survey (NERC) for permission to use the base map employed in Figure 3, Jim Rose and Christine Lane for comments on an earlier draft of this contribution, Dorothy Weston for assistance with field sampling, and Jen Thornton (née Kynaston) for constructing or improving the illustrations. We also owe a debt of gratitude to Colin Ballantyne and Sven Lukas for reviews of the original submitted draft that included astute recommendations leading to the article's improvement. This study is a contribution to the INTIMATE programme ('INTegrating Ice-core, MArine and TErrestrial records for the period 60,000 to 8,000 years ago': http://intimate.nbi.ku.dk ).

## References


Andersen, K.K., Svensson, A., Rasmussen, S.O., Steffensen, J.P., Johnsen, S.J.,Bigler, M., Röthlisberger, R., Ruth, U., Siggaard-Andersen, M.-L., Dahl-Jensen, D., Vinther, B.M., Clausen, H.B., 2006. The Greenland Ice Core Chronology 2005, 15-42 ka. Part 1: constructing the time scale. Quat. Sci. Rev. 25, 3246-3257.

Arosio, R., Howe, J.A., 2018. Lateglacial to Holocene palaeoenvironmental change in the Muck Deep, offshore western Scotland. Scott. J. Geol. 54, 99-114.

Bakke, J., Lie, O., Heegaard, E., Dokken, T., Haug, G.H., Birks, H.H., Dulski, P., and Nilsen, T., 2009, Rapid oceanic and atmospheric changes during the Younger Dryas cold period. Nat. Geosci. 2, 202–205.

Baldini , L.M., McDermott, F., Baldini , J.U.L., Arias, P., Cueto, M., Fairchild, I.J., Hoffmann, D.L., Mattey, D.P., Müller, W., Constantin Nita, D., Ontañón, R., Garciá-Moncó, C., Richards, D.A., 2015. Regional temperature, atmospheric circulation, and sea-ice variability within the Younger Dryas Event constrained using a speleothem from northern Iberia. Earth Planet. Sci. Lett. 419. 101-110.

Ballantyne, C.K., 2007. Loch Lomond Stadial glaciers in North Harris, Outer Hebrides, North-West Scotland: glacier reconstruction and palaeoclimatic implications. Quat. Sci. Rev. 26, 3134-3149.

Ballantyne, C. K., 2012. Chronology of glaciation and deglaciation during the Loch Lomond (Younger Dryas) Stade in the Scottish Highlands: implications of recalibrated $^{10}$Be exposure ages. Boreas 41, 513-526.

Ballantyne, C.K., Small, D., 2019. The last Scottish ice sheet. Earth Env. Sci. Trans. Roy. Soc. Edinb. (in First View).

Ballantyne, C.K., Stone, J.O., 2012. Did large ice caps persist on low ground in northwest Scotland during the Lateglacial Interstade? J. Quat. Sci. 27, 297-306.

Bartolomé, M., Moreno, A., Sancho, S., Stoll, H.M., Cacho, I., Spötl, C., Belmonte, Á., Edwards, R.L., Cheng, H., Hellstrom, J.C., 2015. Hydrological change in Southern Europe responding to increasing North Atlantic overturning during Greenland Stadial 1. Proc. Natl. Acad. Sci. USA 114, 10047-10052.

Benn, D.I. 1997. Glacier fluctuations in western Scotland. Quat. Int. 38-39, 137-147.

Bennike, O., Mortensen, M.F., 2018. A multi-disciplinary macrofossil study of late glacial to early Holocene sediments from Søndre Kobberdam, Hareskovene, Denmark. Bull. Geol. Soc. Denm. 66, 113–122.

Bickerdike, H.L., Evans, D.J.A., Ó Cofaigh, C.O., Stokes, C.R., 2016. The glacial geomorphology of the Loch Lomond Stadial in Britain: a map and geographic information system resource of published evidence. J. Maps 12, doi.org/10.1080/17445647.2016.1145149.

Bickerdike, H.L., Ó Cofaigh, C.O., Evans, D.J.A., Stokes, C.R., 2018a. Glacial landsystems, retreat dynamics and controls on Loch Lomond Stadial (Younger Dryas) glaciation in Britain. Boreas 47, 202-224.

Bickerdike, H.L., Evans, D.J.A., Stokes, C.R., Ó Cofaigh, C.O., 2018b. The glacial geomorphology of the Loch Lomond (Younger Dryas) Stadial in Britain: a review. J. Quat. Sci. 33, 1-54.

Björck, S., Walker, M.J.C., Cwynar, L., Johnsen, S.J., Knudsen, K-L., Lowe, J.J., Wohlfarth, B., INTIMATE Members, 1998. An event stratigraphy for the Last Termination in the North Atlantic region based on the Greenland Ice Core record: a proposal by the INTIMATE group. J. Quat. Sci.13, 283-292.

Bondevik, S., Mangerud, J., 2012. A calendar age estimate of a very late Younger Dryas ice sheet maximum in western Norway. Quat. Sci. Rev.21, 1661-1676.

Böse, M., 1995. Problems of dead ice and ground ice in the central part of the North European Plain. Quat. Int. 28, 123-125.

Boutton, T.W., 1991. Stable carbon isotope ratios of natural materials. II. Atmospheric, terrestrial, marine and freshwater environments. In Coleman, D.C., Fry, B. (eds), *Carbon Isotope Techniques*, Academic Press, San Diego & London, 173-186.

Bowman, S. , 1990. *Radiocarbon Dating.* British Museum, London.

Brauer, A., Hajdas, I., Blockley, S.P.E., Bronk Ramsey, C., Christl, M., Ivy-Ochs, S., Moseley, G., Nowaczyk, N.N., Rasmussen, S.O., Roberts, H., Spötl, C., Staff, R., Svensson, A., 2014. The importance of independent chronology in integrating records of past climate change for the 60-8 ka INTIMATE time interval. Quat. Sci. Rev.106, 47-66.

Bromley, G.R.M., Putnam, A.E., Rademaker, K.M., Lowell, T.V., Schaefer, J.M., Hall, B., Winckler, G., Birkel, S.D., Borns, H.W., 2014. Younger Dryas deglaciation of Scotland driven by warming summer. Proc. Natl. Acad. Sci. USA 111, 6215–6219.

Bromley, G.R.M., Putnam, A.E., Lowell, T.V., Hall, B.L., Schaefer, J.M., 2016. Comment on 'Was Scotland deglaciated during the Younger Dryas?' by Small and Fabel (2016). Quat. Sci. Rev.152, 203-206.

Bromley, G.R.M., Putnam, A., Borns Jr., H., Lowell, T., Sandford, T., Barrell, D., 2018. Interstadial rise and Younger Dryas demise of Scotland's last ice fields. Paleoceanogr. Paleoclimatol. 33, 412-429.

Bronk Ramsey, C., 2009a. Bayesian Analysis of Radiocarbon Dates. Radiocarbon 51, 337-360.

Bronk Ramsey, C., 2009b. Dealing with outliers and offsets in radiocarbon dating. Radiocarbon 51, 1023-1045.

Bronk Ramsey, C., 2017. OxCal project, Version 4.3. Web source from April 2017. https://c14.arch.ox.ac.uk/oxcal/OxCal.html

Bronk Ramsey, C., Lee, S., 2013. Recent and planned developments of the program OxCal. Radiocarbon 55, 720–730.

Bronk Ramsey, C., Albert, P.G., Blockley, S.P., Hardiman, M., Housley, R.A., Lane, C.S., Lee, S., Matthews, I.P., Smith, V.C., Lowe, J.J., 2015. Improved age estimates for key Late Quaternary European tephra horizons in the RESET lattice. Quat. Sci. Rev.118,18–32.

Brooks, S.J., Davies, K.L., Mather, K.A., Matthews, I.P., Lowe, J.J., 2016. Chironomid inferred summer temperatures for the last glacial–interglacial transition from a lake sediment sequence in Muir Park Reservoir, west-central Scotland. J. Quat. Sci.31, 214–224.

Browne, M.A.E., Graham, D.K., 1981. Glaciomarine deposits of the Loch Lomond Stade glacier in the Vale of Leven between Dumbarton and Balloch, west-central Scotland. Quat. Newsl. 34, 1-7.

Chandler, B.M.P., 2018. Extent, style and timing of former glaciation in the Gaick, Central Grampians, Scotland, and implications for palaeoclimate. Unpublished PhD thesis,. Queen Mary University of London, pp. 356.

Chandler, B.M.P., Boston, C.M., Lukas, S., 2019. A spatially-restricted Younger Dryas plateau icefield in the Gaick, Scotland: Reconstruction and palaeoclimatic implications. Quat. Sci. Rev.211, 107-135.

Clark, C.D., Hughes, A.L.C., Greenwood, S.L., Jordan, C. & Sejrup, H.P., 2012. Pattern and timing of retreat of the last British-Irish ice sheet. Quat. Sci. Rev.44, 112-146.

Davies, S.M., Wastegård, S., Wohlfarth, B., 2003. Extending the limits of the Borrobol Tephra to Scandinavia and detection of new early Holocene tephras. Quat. Res. 59, 345–352.

Eynaud, F., de Abreu, L., Voelker, A., Schönfeld, J., Salgueiro, E., Turon, J.-L., Penaud, A., Toucanne, S., Naughton, F., Sánchez-Goñi, M.F., Malaizé, B., Cacho, I., 2009. Position of the Polar Front along the western Iberian margin during key cold episodes of the last 45 ka. Geochem., Geophys., Geosys. 10, 21 pp. (10.1029/2009GC002398).

Farnsworth, W.R., Ingólfsson, Ó., Retelle, M., Allaart, L., Håkansson, L.M., Schomacker, A., 2018. Svalbard glaciers re-advanced during the Pleistocene–Holocene transition. Boreas 47, 1022-1032.

Finlayson, A., Golledge, N., Bradwell, T.,Fabel, D., 2011. Evolution of a Lateglacial mountain icecap in northern Scotland. Boreas 40, 536-554.

Golledge, N.R., 2007. An ice cap landsystem for palaeoglaciological reconstructions: characterizing the Younger Dryas in western Scotland. Quat. Sci. Rev. 26, 213-229.

Golledge, N.R., 2010. Glaciation of Scotland during the Younger Dryas stadial: a review. J. Quat. Sci. 25, 550–566.

Golledge, N.R., Hubbard, A.L., Sugden, D.E., 2009. Mass balance, flow and subglacial processes of a modelled Younger Dryas ice cap in Scotland. J. Glaciol. 55, 32-42.

Golledge, N. R., Hubbard, A., Sugden, D. E., 2008. High-resolution numerical simulation of Younger Dryas glaciation in Scotland. Quat. Sci. Rev. 27, 888–904.

Gray, J.M., Brooks, C.L., 1972. The Loch Lomond Readvance moraines of Mull and Menteith. Scott. J. Geol. 8, 95-103.

Gray, J.M., Lowe, J.J., 1977. The Scottish Lateglacial environment: a synthesis, In J.M. Gray & J.J. Lowe (eds.), *Studies in the Scottish Lateglacial Environment*, Pergamon, Oxford, 163-181.

Gulliksen, S., Birks, H.H. Possnert, G., Mangerud, J., 1998. A calendar age estimate of the Younger Dryas-Holocene boundary at Kråkenes, western Norway. The Holocene 8, 249-259.

Ham, N.R. & Attig, J., 1996. Ice wastage and landscape evolution along the southern margin of the Laurentide Ice Sheet, north-central Wisconsin. Boreas 25, 171-186.

Henriksen, M., Mangerud, J., Matiouchkov, A., Paus, A. & Svendsen, J.I., 2003. Lake stratigraphy implies an 80,000 yr delayed melting of buried dead ice in northern Russia. J. Quat. Sci.18, 663-679.

Hinxman, L.W., Carruthers, R.G. and Macgregor, M. , 1923. The geology of Corrour and the Moor of Rannoch. Mem. Geol. Surv. Scotland.

Hornsey, J., 2016. Combined use of high resolution remote sensing and field mapping to determine ice-flow dynamics on Rannoch Moor, Scotland, during the Loch Lomond Stadial. Unpublished MSc dissertation, Royal Holloway, University of London.

Jochum, K.P., Stoll, B., Herwig, K., Willbold, M., Hofmann, A.W. et al., 2006. MPI-DING reference glasses for in situ microanalysis: new reference values for element concentrations and isotope ratios. Geochem. Geophys. Geosys. 7, http://dx.doi.org/10.1029/2005GC001060.

Jones, G., Davies, S.M., Farr, G.J., Bevan, J., 2017. Identification of the Askja-S Tephra in a rare turlough record from Pant-y-Llyn, south Wales. Proc. Geol. Assoc. 128 (4), 523-530.

Kearney, R., Albert, P.G., Staff, R.A., Pal, I., Veres, D., Magyari, E., Bronk Ramsey, C., 2018. Ultra-distal fine ash occurrences of the Icelandic Askja-S Plinian eruption deposits in Southern Carpathian lakes: New age constraints on a continental scale tephrostratigraphic marker. *Quat. Sci. Rev.*188, 174-182.

Kelly, T.J., Hardiman, M., Lovelady, M., Lowe, J.J., Blockley, S.P.E., 2017. Scottish early Holocene vegetation dynamics based on pollen and tephra records from Inverlair and Loch Etteridge, Inverness-shire. Proc. Geol. Assoc. 128, 125-135.

Lane, C.S., Blockley, S.P.E., Bronk Ramsey, C., Lotter, A.F., 2011. Tephrochronology and absolute centennial scale synchronisation of European and Greenland records for the last glacial to interglacial transition: a case study of Soppensee and NGRIP. Quat. Int. 246, 145–156.

Lane, C.S., De Klerk, P., Cullen, V.L., 2012. A tephrochronology for the Lateglacial palynological record of the Endinger Bruch (Vorpommern, north-east Germany). J. Quat. Sci. 27, 141–149.

Lane, C.S., Brauer, A., Blockley, S.P.E. & Dulski, P. 2013., Volcanic ash reveals time-transgressive abrupt climate change during the Younger Dryas. Geology 41, 1251-1254.

Lilja, C., Lind, E.M., Morén, B., Wastegård, S., 2013. A Lateglacial-early Holocene tephrochronology for SW Sweden. Boreas 42, 544–554.

Lind, E.M., Wastegård, S., 2011. Tephra horizons contemporary with short early Holocene climate fluctuations: new results from the Faroe Islands. Quat. Int. 246, 157–167.

Lowe, J., Hoek, W., INTIMATE Group, 2001. Inter-regional correlation of palaeoclimatic records for the Last Glacial-Interglacial Transition: a protocol for improved precision recommended by the INTIMATE project group. Quat. Sci. Rev. 20, 1175-1187.

Lowe, J. J., Palmer, A.P., Carter-Champion, A., MacLeod, A. M., Ramírez-Rojas, I., Timms, R. G. O., 2017. Stratigraphy of Lateglacial lake sediments at Turret Bank, Upper Glen Roy, Lochaber: implications for the age of the Turret Fan. Proc. Geol. Assoc.128, 110-124.

Lowe, J.J., Walker, M.J.C., 1976. Radiocarbon dates and deglaciation of Rannoch Moor, Scotland. Nature 264, 632-633.

Lowe, J.J. & Walker, M.J.C., 1979. Pollen analyses, radiocarbon dates and the deglaciation of Rannoch Moor, Scotland, following the Loch Lomond Advance. In R.A. Cullingford et al. (eds.), *Timescales in Geomorphology*, Wiley, London & New York, 247 259.

Lowe, J.J., Walker, M.J.C., 1980. Problems with radiocarbon dating the close of the Lateglacial period in the Rannoch Moor area, Scotland. In: Lowe, J.J., Gray, J.M., Robinson, J.E. (Eds.), *Studies in the Lateglacial of North West Europe*. Pergamon Press, Oxford, pp. 123-131.

Lowe, J.J., Walker, M.J.C., 2000. Radiocarbon dating the last glacial-interglacial transition (ca. 14-9 14C ka BP) in terrestrial and marine records: the need for new quality assurance protocols. Radiocarbon 42, 53-68.

Lukas, S., Bradwell, T., 2010. Reconstruction of a Lateglacial (Younger Dryas) mountain ice field in Sutherland, northwestern Scotland, and its palaeoclimatic implications. J. Quat. Sci. 25, 567-580.

MacDonald, G.M., Beukens, R.P., Kieser, W.E., Vitt, D.H., 1987. Comparative radiocarbon dating of terrestrial plant macrofossils and aquatic moss from the “ice-free corridor” of western Canada. Geology, 15, 837-840.

MacLeod, A., Palmer, A., Lowe, J., Rose, J., Bryant, C., Merritt, J., 2011. Timing of glacier response to Younger Dryas climatic cooling in Scotland. Glob. Planet. Change, 264-274.

MacLeod, A., Matthews, I.P., Lowe, J.J., Palmer, A.P., Albert, P.G., 2015. A second tephra

isochron for the Younger Dryas period: the Abernethy Tephra. Quat. Geochron. 28, 1–11.

Mangerud, J., Aarseth, I., Hughes, A.L.C., Lohne, Ø.S., Skår, K., Sønstegaard, E., Svendsen, J.I., 2016. A major re-growth of the Scandinavian Ice Sheet in western Norway during Allerød-Younger Dryas. Quat. Sci. Rev.132, 175-205.

Mangerud, J., Andersen, S.Th., Berglund, B.E., Donner, J.J., 1974. Quaternary stratigraphy of Norden: a proposal for terminology and classification. Boreas 3, 109-128.

Mangerud, J., Hughes, A.L.C., Saele, T.H., Svendsen, J.I., 2019. Ice-flow patterns and precise timing of ice sheet retreat across a dissected fjord landscape in western Norway. Quat. Sci. Rev. 214, 139-163.

Marty, J., Myrbo, A., 2014. Radiocarbon dating suitability of aquatic plant macrofossils. J. Paleolim. 52, 435-443.

Matthews, I.P. Birks, H.H., Bourne, A., Brooks, S.J., Lowe, J.J., MacLeod, A. & Pyne-O'Donnell, S.D.F., 2011. New age estimates and climatostratigraphic correlations for the Borrobol and Penifiler tephras: evidence from Abernethy Forest, Scotland. J. Quat. Sci. 26, 247-252.

Merritt J.W., Coope G.R., Taylor B.J., Walker M.J.C., 1990. Late Devensian organic deposits beneath till in the Teith Valley, Perthshire. Scott. J. Geol. 26,15–24.

Mix, A.C., Fairbanks, R.G., 1985. North Atlantic surface-ocean control of Pleistocene deep-ocean circulation. Earth Planet. Science. Lett. 73, 231-243.

Nielson, J.C., Kokelaar, B.P., Crowley, Q.G., 2009. Timing, relations and cause of plutonic and volcanic activity of the Siluro-Devonian post-collision magmatic episode in the Grampian Terrane, Scotland. J. Geol. Soc. London 166, 545-561.

Neugeberger, I., Brauer, A., Dräger, N., Dulski, P., Wulf, S., Plessen, B., Mingram, J., Herzschuh, U., Brande, A., 2012. A Younger Dryas varve chronology from the Rehwiese palaeolake record in NE-Germany. Quat. Sci. Rev. 36, 91-102.

Ott, F., Wulf, S., Serb, J., Słowiński, M., Obremska, M., Tjallingii, R., Błaszkiewicz, M., Brauer, A., 2016. Constraining the time span between the early Holocene Hässeldalen and Askja-S tephras through varve counting in the Lake Czechowskie sediment record, Poland. J. Quat. Sci. 31, 103–113.

Palmer, A.P., Lowe, J.J., 2017. Dynamic landscape changes in Glen Roy and vicinity, west Highland Scotland, during the Last Termination: a synthesis. Proc. Geol. Assoc. 128, 2-25.

Palmer, A.P., Rose, J., Lowe, J.J., MacLeod, A., 2010. Annually-resolved events of Younger Dryas glaciation in Lochaber (Glen Roy and Glen Spean), Western Scottish Highlands. J. Quat. Sci. 25, 581-596.

Palmer, A.P., Rose, J., Rasmussen, S.O., 2012. Evidence for phase-locked changes in climate between Scotland and Greenland during GS-1 (Younger Dryas) using micromorphology of glaciolacustrine varves from Glen Roy. Quat. Sci. Rev. 36, 114–123.

Peacock, J.D., 1971. Marine shell radiocarbon dates and the chronology of deglaciation in western Scotland. Nature 230, 43−45.

Peacock, J.D., Graham D.K., Wilkinson, I.P., 1978. Late-glacial and post-glacial marine environments at Ardyne, Scotland, and their significance in the interpretation of the history of the Clyde Sea Area. Rep. Inst. Geol. Sci. 80/7.

Peacock, J.D., Harkness, D.D., Housley, R.A., Little, J.A., Paul, M.A., 1989. Radiocarbon ages for a glaciomarine bed associated with the maximum of the Loch Lomond Readvance in west Benderloch, Argyll. Scott. J. Geol. 25, 69−79.

Peacock, J.D., Rose, J., 2017. Was the Younger Dryas (Loch Lomond Stadial) icefield on Rannoch Moor, western Scotland, deglaciated as early as c.12.5 cal ka BP? Proc. Geol. Assoc. 128, 173-179.

Pilcher, J., Bradley, R.S., Francus, P., Anderson, L., 2005. A Holocene tephra record from the Lofoten Islands, Arctic Norway. Boreas 34, 136–156.

Putnam, A.E., Bromley, G.R.M., Rademaker, K., Schaefer, J.M., 2019. In situ $^{10}$Be production-rate calibration from a $^{14}$C-dated late-glacial moraine belt in Rannoch Moor, central Scottish Highlands. Quat. Geochron. 50, 109-125.

Rach, O., Brauer, A., Wilkes, H., Sachse, D., 2014. Delayed hydrological response to Greenland cooling at the onset of the Younger Dryas in western Europe. Nature Geosci. 7, 109-112.

Rasmussen, S.O., Andersen, K.K., Svensson, A.M., Steffensen, J.P., Vinther, B.M., Clausen, H.B., Siggaard-Andersen, M.-L., Johnsen, S.J., Larsen, L.B., Dahl- Jensen, D., Bigler, M., Röthlisberger, R., Fischer, H., Goto-Azuma, K., Hansson, M.E., Ruth, U., 2006. A new Greenland ice core chronology for the last glacial termination. J. Geophys. Res.111, D06102.

Rasmussen, S.O., Bigler, M., Blockley, S.P.E., Blunier, T, Buchardt, S.L., Clausen, H.B., Cvijanovic, I., Dahl-Jensen, D., Johnsen, S.J., Fischer, H., Gkinis, V., Guillevic, M., Hoek, W.Z., Lowe, J.J., Pedro, J., Popp, T., Seierstad, I.K., Steffensen, J.P., Svensson, A., Vallelonga, P., Vinther, B.M., Walker, M.J.C., Wheatley, J.J &, Winstrup, M., 2014. A stratigraphic framework for abrupt climatic changes during the last glacial period based on three synchronised Greenland ice-core records: refining and extending the INTIMATE event stratigraphy. Quat. Sci. Rev.106, 14-28.

Reimer, P. J., Bard, E., Bayliss, A. Beck, J. W., Blackwell, P. G., Bronk Ramsey, C., Buck, C. E., Cheng, H., Edwards, R. L., Friedrich, M., Grootes, P. M., Guilderson, T. P., Haflidason, H., Hajdas, I., Hatte´, C., Heaton, T. J., Hoffman, D. L., Hogg, A. G., Hughen, K. A., Kaiser, K. F., Kromer, B., Manning, S. W., Niu, M., Reimer, R. W., Richards, D. A., Scott, E. M., Southon, J. R., Staff, R. A., Turney, C. S. M. & van der Plicht, J., 2013. IntCal13 and Marine 13 radiocarbon age calibration curves 0–50,000 years cal. BP. Radiocarbon 55, 1869–87.

Romundset, A., Lakeman, T.R., Høgaas, F., 2019. Coastal lake records add constraints to the age and magnitude of the Younger Dryas ice-front oscillation along the Skagerrak coastline in southern Norway. J. Quat. Sci. 34, 112-124.

Rose, J., 1981. Field Guide to the Quaternary Geology of the South Eastern part of the Loch Lomond Basin: Glasgow. Proc. Geol. Soc. Glasgow 122/123, 12–28.

Rose, J., Lowe, J.J., Switsur, R.V., 1988. A radiocarbon date on plant detritus beneath till from the type area of the Loch Lomond Readvance. Scott. J. Geol. 24,113–124.

Rossi, B., Bajo, P., Lozano, R.P., Hellstrom, J., 2018. Younger Dryas to Early Holocene paleoclimate in Cantabria (N. Spain): Constraints from speleothem Mg, annual fluorescence banding and stable isotope records. Quat. Sci. Rev. 192, 71-85.

Ruddiman, W.F., McIntyre, A., 1976. The North Atlantic palaeoclimatic changes over the past 600,000 years. Geol. Soc. Amer. Mem. 145, 111-146.

Ruddiman, W.F., McIntyre, A., 1981. The North Atlantic during the last deglaciation. Palaeogeogr. Palaeoclimatol. Palaeoecol. 35, 145-214.

Sarafis, V., 1971. A biological account of *Polytrichum commune*. New Zealand J. Bot. *9*, 711-724.

Sigvaldason, G.E., 2002. Volcanic and tectonic processes coinciding with glaciation and crustal rebound: an early Holocene rhyolitic eruption in the Dyngjufjöll volcanic centre and the formation of the Askja caldera, north Iceland. Bull. Volcanol. 64, 192-205.

Simpson, J.B.. 1933. The late-glacial readvance moraines of the Highland border west of the River Tay. Trans. R. Soc. Edinb. 61, 687-698.

Sissons, J.B., 1967. Glacial stages and radiocarbon dates in Scotland. Scott. J. Geol. 3, 375-381.

Sissons, J.B., 1974. The Quaternary in Scotland: a review. Scott. J. Geol. 10, 311−337.

Sissons, J.B., 1979a. The later lakes and associated fluvial terraces of Glen Roy Glen Spean and vicinity. Trans. Inst. Brit. Geogr. 4, 12–29.

Sissons, J.B., 1979b. Catastrophic lake drainage in Glen Spean and the Great Glen, Scotland. J. Geol. Soc. London 136, 215–224.

Sissons, J.B., 2017. The Lateglacial lakes of Glen Roy, Spean and vicinity (Lochaber District, Scottish Highlands). Proc. Geol. Assoc.128, 32–41.

Small, D., Fabel, D., 2016a.Was Scotland deglaciated during the younger Dryas? Quat. Sci. Rev. 145, 259-263.

Small, D., Fabel, D., 2016b. Response to Bromley et al. "Comment on 'Was Scotland deglaciated during the Younger Dryas?' By Small and Fabel (2016). Quat. Sci. Rev.152, 206-208.

Smith, C.G., Marsden, G.R., 1977. Report on geophysical and geological survey at Blackmount, Argyllshire. Mineral Reconnaissance Progress Report No. *16*, Natural Environment Research Council, UK (10 pp.).

Stephenson, D., Mendum, J.R., Fettes, D.J., Leslie, A.G., 2013. The Dalradian rocks of Scotland: an introduction. Proc. Geol. Assoc. 124, 3-82.

Sutherland, D.G., 1981. The raised shorelines and deglaciation of the Loch Long/Loch Fyne area, western Scotland. Unpublished PhD thesis, University of Edinburgh.

Sutherland D.G., 1984. The Quaternary deposits and landforms of Scotland and the neighbouring shelves: a review. Quat. Sci. Rev. 3, 157–254.

Sutherland, D.G., 1986. A review of Scottish marine shell radiocarbon dates, their standardization and interpretations. *Scott. J. Geol.* 22, 145−164.

Sveinsbjörndóttir, A.E., Heinemeier, J., Rud, N., Johnsen, S.J., 1992. Radiocarbon anomalies observed for plants growing in Icelandic geothermal waters. Radiocarbon 34, 696-703.

Svensson, A., Andersen, K.K., Bigler, M., Clausen, H.B., Dahl-Jensen, D., Davies, S.M.,Johnsen, S.J., Muscheler, R., Parrenin, F., Rasmussen, S.O., Röthlisberger, R.,Seierstad, I., Steffensen, J.P., Vinther, B.M., 2008. A 60,000 year Greenland stratigraphic ice core chronology. Clim. Past 4, 47-57.

Thorp, P.W., 1991. Surface profiles and basal shear stresses of outlet glaciers front a Late-glacial mountain ice field in western Scotland. J. Glaciol. 125, 77-88.

Timms, R.G.O., 2016. Developing a refined tephrostratigraphy for Scotland, and constraining abrupt climatic oscillations of the Last Glacial-Interglacial Transition (ca 16-8 ka BP) using high resolution tephrochronologies. Unpublished PhD thesis, University of London.

Timms, R.G.O., Matthews, I.P., Palmer, A.P., Candy, I. & Abel, L., 2017. A high-resolution tephrostratigraphy from Quoyloo Meadow, Orkney, Scotland: implications for the tephrostratigraphy of NW Europe during the Last Glacial-Interglacial Transition. Quat. Geochron. 40, 67-81.

Timms, R.G.O., Matthews, I.P., Palmer, A.P., Candy, I., 2018. Toward a tephrostratigraphic framework for the British Isles: a Last Glacial to Interglacial Transition (LGIT c. 16-8 ka) case study from Crudale Meadow, Orkney. Quat. Geochron. 46, 28-44.

Timms, R.G.O., Matthews, I.P., Lowe, J.J., Palmer, A.P., Weston, D.J., MacLeod, A., Blockley, S.P.E., 2019. Establishing tephrostratigraphic frameworks to aid the study of abrupt climatic and glacial transitions: A case study of the Last Glacial-Interglacial Transition in the British Isles (c. 16-8 ka BP). Earth-Sci. Rev. 192, 34-64.

118.Turney, C.S.M., Van Den Burg, K., Wastegård, S., Davies, S.M., Whitehouse, N.J., Pilcher, J.R., Callaghan, C., 2006. North European last glacial-interglacial transition (LGIT; 15-9 ka) tephrochronology: extended limits and new events. J. Quat. Sci. 21, 335–345.

Walker, M.J.C., Björck, S., Lowe, J.J., Cwynar, L., Johnsen, S., Knudsen, K-L., Wohlfarth, B., INTIMATE group, 1999. Isotopic 'events' in the GRIP ice core: a stratotype for the Late Pleistocene. Quat. Sci. Rev.18, 1143–1150.

Walker, M.J.C., Björck, S. & Lowe, J.J., 2001. Integration of ice core, marine and terrestrial records (INTIMATE) from around the North Atlantic region: an introduction. Quat. Sci. Rev. 20, 1169-1174.

Walker, M.J.C., Lowe, J.J., 1977. Postglacial environmental history of Rannoch Moor, Scotland. I. Three pollen diagrams from the Kingshouse area. J. Biogeogr. 4, 333-351.

Walker, M.J.C., Lowe, J.J., 1979. Postglacial environmental history of Rannoch Moor, Scotland. II. Pollen diagrams and radiocarbon dates from the Rannoch Station and Corrour areas. J. Biogeogr. 6, 349-362.

Walker, M.J.C., Lowe, J.J., 1981. Postglacial environmental history of Rannoch Moor, Scotland. III. Early and mid-Flandrian pollen-stratigraphic data from sites on western Rannoch Moor and near Fort William. J. Biogeogr. 8, 475-491.

Walker, M.J.C., Lowe, J.J., 2019. Lateglacial environmental change in Scotland. Earth Env. Sci. Trans. R. Soc. Edinb. (in First View).

Watson, E.V., 1981. *British Mosses and Liverworts* (3rd ed.). Cambridge University Press.

Wohlfarth,B., Luoto,T.P., Muschitiello,F.,Väliranta, M., Björck,S.,Davies,S. M., Kylander, M., Ljung, K., Reimer, P. J., Smittenberg, R. H., 2018. Climate and environment in southwest Sweden 15.5–11.3 cal. ka BP. Boreas 47, 687-710.

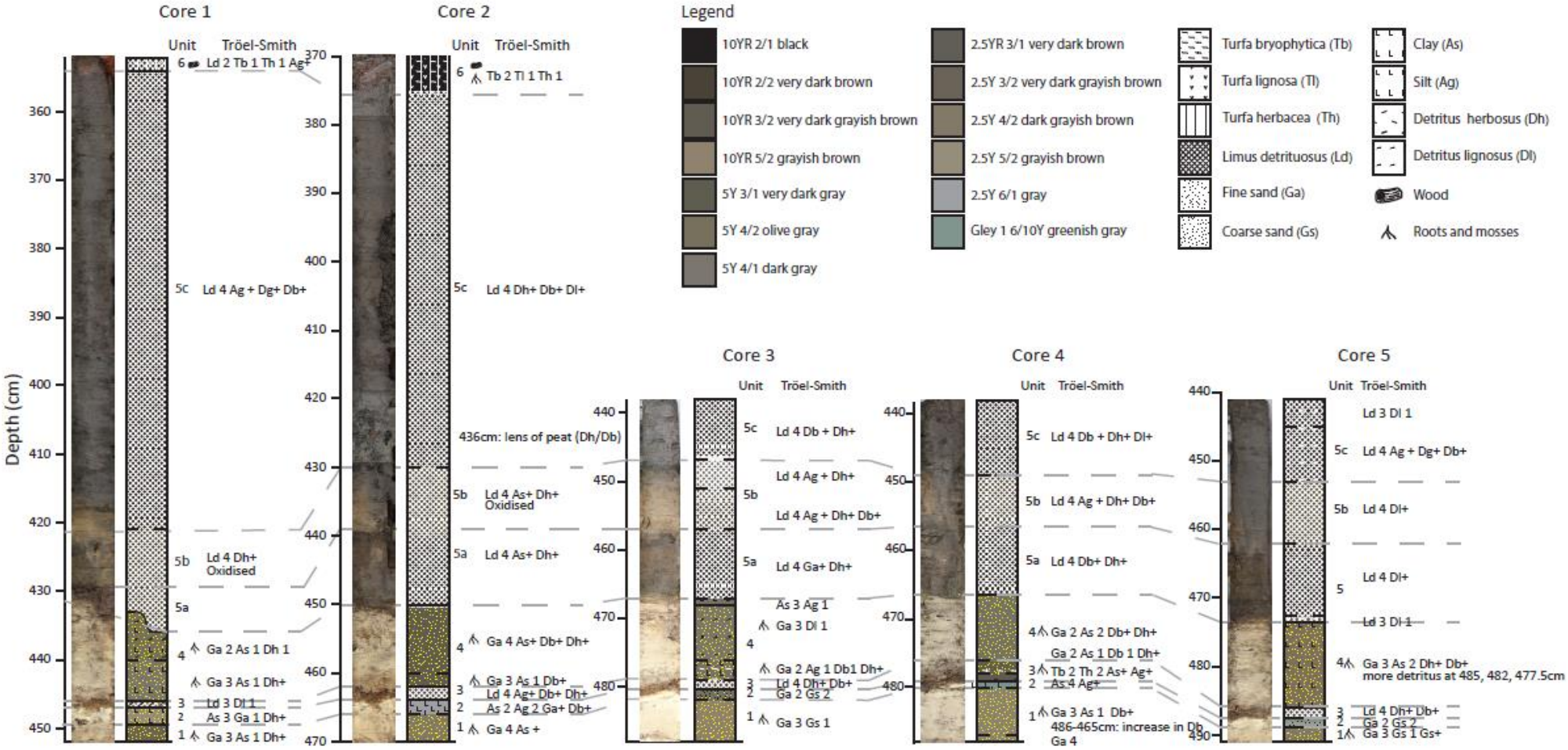


**Appendix A.** Images and descriptions of the lithostratigraphic units observed in five cores obtained from the Kingshouse 2 basal sedimentary sequence; note the clear consistency in the sequences of lithological units 1 to 5c and their boundaries.

***Appendix B*:** Field and laboratory methods

## B.1 Field methods

The site was initially sounded at regular rectilinear intervals to establish the deepest part of the basin, which was found to be a relatively narrow zone (~3 $m^2$). Sediment cores were recovered from this part of the basin using a Russian coring device with chambers of one-metre and 50-cm length and an internal diameter of 5 cm. Cores were collected within close proximity to each other, which resulted in the maintenance of comparable lithostratigraphic sequences (**Appendix A**). The recovered sediment cores were transferred into semi-circular plastic guttering, sealed in clear waterproof adhesive to preserve delicate sedimentary structures and to avoid contamination and compression of the soft lake muds, and stored at all times in a cold store with a controlled temperature below 4°C.

## B.2 Sediment description

Sediment descriptions (**Appendix A**) follow the Tröels-Smith (1955) classification system and Munsell colour scheme. The cores were cleaned using horizontal strokes, to avoid vertical transfer of contaminating material. Magnetic susceptibility variations were measured at 1-cm intervals using a Bartington MS2 meter and MS2 C core logging sensor (65 mm diameter). Sediment samples were extracted at 1-cm contiguous vertical intervals for loss-on-ignition (LOI) measurement over the lower 50 cm of core 2 and the entire 1 metre length of core 3. Samples were dried overnight at 105°C, weighed for the dry sediment mass (α), incinerated at 550°C for two hours and weighed for the ash sediment mass (β). The ashed samples were retained and examined for tephra content in those intervals in which analysis at 1-cm vertical intervals was deemed necessary.

## B.3 Pollen analysis

Contiguous sample aliquots of measured 1 $cm^3$ volume were extracted from the organic sediments in the lower 50 cm of core 2, but increased to 2 $cm^3$ in the lower minerogenic units, to increase the

prospect of securing countable amounts of pollen grains. Samples were deflocculated in sodium pyrophosphate ($Na_4P_2O_7$). Exotic *Lycopodium* tablets, containing a known number of spores, were added to enable the estimation of pollen concentration. The deflocculated samples were sieved using 125 μm and 10 μm meshes. <5ml of 10% Hydrochloric acid (HCl) was added to the samples to remove calcium carbonate. Samples were floated using sodium polytungstate ($3Na_2WO_4.9WO_3$) at a density of 2.0 g $cm^{-3}$ to separate pollen grains from the host sediment. The residues were treated using Erdtman's acetolysis, involving the application of a 9:1 mixture of acetic anhydride ($(CH_3CO)_2O$) and sulphuric acid ($H_2SO_4$) to remove biological cellulose. The resultant residues were rinsed in deionised water and mounted on standard optical microscope slides using glycerol gel. Of the 34 pollen samples analysed, minimum counts of 300 total land pollen (TLP) were achieved for all but five samples; the lower counts ranged from 101 to 203 TLP, and were samples obtained from the coarse minerogenic sediments near the base of the sequence. Below 464 cm depth, the sediments were nearly devoid of pollen and spores.

### B.4 Tephrostratigraphy

Contiguous sediment samples of 1 $cm^3$ were cut from Cores 2 and 3 and treated using the laboratory procedures of Turney et al. (1998) with the modifications of Blockley et al. (2005). Sieve meshes of 125 μm and 15 μm size were employed to reduce the sediment particle size range. The resulting residues were immersed first in sodium polytungstate (SPT) solution of density 1.95 g $cm^{-3}$ to remove organic material, the residues subsequently being immersed in SPT of density 2.55 g $cm^{-3}$ to separate glass shards from the host deposits by floatation. The resulting extraction floats were mounted on standard optical microscope slides using Canada Balsam. Tephra shards were counted using a polarising Olympus CH2 light microscope at 100X and 400X magnifications. Samples found to contain shards were re-sampled and prepared for geochemical analysis repeating the above procedures, but adding teepol/0.5% sodium hexametaphosphate to ease the separation process, when

necessary. Extraction floats were examined under a polarising light microscope at 100X magnification and shards extracted using a micromanipulator, which were placed on a silicon square, sealed using a Specifix-40 resin 'stub', and cured at 50°C for 3.5 hours. The shard surfaces were subsequently exposed using P2500 and P4000 grinding papers with a final polish using 0.3μm aluminium oxide powder and MasterTex paper. Stubs analysed at Oxford University were measured using a JEOL JXA-8600 superprobe electron microprobe (EPMA WDS) with a beam current of 6nA, accelerating voltage of 15 kV and an operating beam diameter of 10 μm. MPI-DING laboratory standards were employed to test for instrumental drift during the analytical runs. Samples measured at the Tephra Analysis Unit at Edinburgh University were analysed using a Cameca SX-100 WDS-EPMA with a 15 keV set at a diameter of 5 μm; a beam current of 2 nA was employed for Na, Al, Si, Fe, K, Ca, Mg and one of 80 nA for F, Mn, Cl and Ti (Hayward, 2012). Machine precision and drift was assessed by the analysis of internal Lipari and BCR-2G secondary standards. All of the geochemical measurements obtained (**Appendix B3, B4**) were filtered using expected ranges of composition to remove values reflecting low quality data, mineral grains and biogenic silica. This ensured only vitreous glass was analysed further. The filtered data were analysed using GeoChemical Data toolkit v3.00 (GCDkit) (Janoušek et al., 2006).

### B.5 Plant macrofossil sample preparation and radiocarbon pretreatment methodology

In the laboratories of the Centre for Quaternary Research, Royal Holloway, sediment samples selected for extraction of plant macrofossil remains were soaked and disaggregated in deionised water and filtered through a sieve of mesh size 125 μm to remove clay particles; this step was repeated if necessary, until the material retained in the sieve was sufficiently disaggregated and cleansed to allow macrofossil remains to be easily separated and identified. The sieved residues were immersed in deionised water in a clock glass and examined under low power magnification. Identifiable macrofossil remains were retrieved individually using a pipette, and stored in deionised

water to which a few drops of dilute (10%) HCl had been added, to prevent bacterial activity during storage and onward transfer to the radiocarbon laboratory. Aquatic species were selectively removed from all samples for the reasons outlined in the main text (i.e. the potential for a reservoir effect leading to inbuilt age). Mosses were also selectively removed from samples except, as noted in the main text, in two cases (467-466cm and 451-450 cm) where moss was purposefully incorporated as a minor component of the sample in order to provide sufficient material for dating. Moreover, in the case of two other sample intervals (464-462cm and 463-461cm depths) where there was sufficient material to do so, pure moss sub-samples were purposefully isolated for dating alongside wholly terrestrial sub-samples from the same depth intervals, in order to provide a direct comparison and hence a test of the potential for inbuilt age associated with moss remains.

Subsequent chemical pretreatment for accelerator mass spectrometry (AMS) radiocarbon dating was performed at the Oxford Radiocarbon Accelerator Unit (ORAU), University of Oxford, UK, using the pretreatment and analytical procedures outlined by Brock et al. (2010). As at most other radiocarbon laboratories, chemical pretreatment generally consists of successive acid-base-acid (ABA) rinses. The three main stages of this process are respectively intended to remove: (i) sedimentary and other carbonate contaminants (a key issue for minimising the risk of inbuilt age from samples growing in a carbonate-rich catchment); (ii) organic (principally humic- and fulvic-) acid contaminants; and (iii) any dissolved atmospheric $CO_2$ that might have been absorbed during the preceding base wash. At ORAU, ABA chemical pretreatment of delicate plant macrofossil samples (laboratory pre-treatment code 'VV') involves successive 1 M HCl (20 mins, 80 °C), 0.2 M NaOH (20 mins, 80 °C) and 1 M HCl (1 hr, 80 °C) washes, with each stage followed by rinsing (≥3 times) with ultrapure MilliQ™ deionised water. Appropriate 'known age' (i.e. independently dendro-chronologically-dated tree-ring) standards are run alongside the unknown age plant macrofossil samples (Staff et al. 2014 ).

Samples were subsequently freeze-dried, weighed into tin capsules, and combusted in an elemental analyser. The $CO_2$ produced is split such that 2% is used for $\delta^{13}C$ (‰) isotope ratio mass spectrometry (IRMS) measurement, with the remaining 98% of $CO_2$ cryogenically frozen into a graphitisation rig and heated at 560ºC for 6 hours in the presence of an iron powder catalyst. The resultant graphite is pressed into aluminium cathodes prior to AMS radiocarbon dating on the 2.5 MV HVEE tandem AMS system at ORAU (Bronk Ramsey et al. 2004 ).

**References**

Brock., F., Higham, T., Ditchfield, P., Bronk Ramsey, C. 2010. Current pre-treatment methods for AMS radiocarbon dating at the Oxford Radiocarbon Accelerator Unit (ORAU). Radiocarbon 52 (1), 103-112.

Bronk Ramsey, C., Higham, T., Leach, P. 2004. Towards high-precision AMS: progress and limitations. Radiocarbon 46 (1), 17-24.

Staff, R.A., Reynard, L., Brock, F. Bronk Ramsey, C. 2014. Wood Pretreatment Protocols and Measurement of Tree-Ring Standards at the Oxford Radiocarbon Accelerator Unit (ORAU). Radiocarbon 56 (2), 709-715.

Tröels-Smith, J. 1955. Characterisation of unconsolidated sediments. *Danmarks Geologiske Undersøgelse*, *Series IV, 3,* 38-73.

Turney, C.S.M. 1998. Extraction of rhyolitic component of Vedde microtephra from minerogenic lake sediments. *Journal of Paleolimnology* 19, 199–206.

| Sample depth | $SiO_2$ | $TiO_2$ | $Al_2O_3$ | $FeO_t$ | MnO | MgO | CaO | $Na_2O$ | $K_2O$ | $P_2O_5$ | Total |
|---|---|---|---|---|---|---|---|---|---|---|---|
| KH2-443 | 73.83 | 0.29 | 11.95 | 2.35 | 0.09 | 0.24 | 1.45 | 4.08 | 2.63 | 0.06 | 96.97 |
| KH2-443 | 73.06 | 0.30 | 11.40 | 2.52 | 0.08 | 0.25 | 1.63 | 4.34 | 2.45 | 0.04 | 96.07 |
| KH2-443 | 72.68 | 0.29 | 11.74 | 2.89 | 0.10 | 0.24 | 1.59 | 4.47 | 2.51 | 0.05 | 96.56 |
| KH2-443 | 74.29 | 0.30 | 11.59 | 2.68 | 0.09 | 0.21 | 1.51 | 4.19 | 2.61 | 0.05 | 97.52 |
| KH2-443 | 73.99 | 0.30 | 11.81 | 2.45 | 0.09 | 0.19 | 1.57 | 4.38 | 2.57 | 0.05 | 97.39 |
| KH2-443 | 72.57 | 0.30 | 11.98 | 2.54 | 0.09 | 0.24 | 1.45 | 4.18 | 2.50 | 0.05 | 95.90 |
| KH2-443 | 73.21 | 0.30 | 11.75 | 2.51 | 0.09 | 0.28 | 1.57 | 4.17 | 2.58 | 0.05 | 96.50 |
| KH2-443 | 72.90 | 0.29 | 11.78 | 2.91 | 0.10 | 0.23 | 1.58 | 4.26 | 2.46 | 0.05 | 96.54 |
| KH2-443 | 73.32 | 0.30 | 11.84 | 2.50 | 0.09 | 0.20 | 1.53 | 4.16 | 2.45 | 0.04 | 96.43 |
| KH2-443 | 73.29 | 0.29 | 11.34 | 2.46 | 0.09 | 0.27 | 1.54 | 4.18 | 2.55 | 0.04 | 96.06 |
| KH2-443 | 71.64 | 0.29 | 11.95 | 2.47 | 0.09 | 0.25 | 1.52 | 4.57 | 2.45 | 0.05 | 95.28 |
| KH2-443 | 73.44 | 0.30 | 11.59 | 2.46 | 0.09 | 0.26 | 1.47 | 4.34 | 2.54 | 0.04 | 96.55 |
| KH2-443 | 71.95 | 0.29 | 10.86 | 2.72 | 0.10 | 0.22 | 1.53 | 4.51 | 2.54 | 0.05 | 94.76 |
| KH2-443 | 72.86 | 0.29 | 11.70 | 2.57 | 0.09 | 0.25 | 1.52 | 4.38 | 2.45 | 0.05 | 96.16 |
| KH2-443 | 71.65 | 0.30 | 11.83 | 2.64 | 0.09 | 0.22 | 1.58 | 4.42 | 2.33 | 0.05 | 95.09 |
| KH2-443 | 72.79 | 0.29 | 11.73 | 2.61 | 0.09 | 0.23 | 1.61 | 4.25 | 2.46 | 0.05 | 96.11 |
| KH2-443 | 73.14 | 0.30 | 11.87 | 2.57 | 0.07 | 0.20 | 1.64 | 4.35 | 2.49 | 0.05 | 96.68 |
| KH2-443 | 72.48 | 0.29 | 11.92 | 2.60 | 0.08 | 0.22 | 1.62 | 4.43 | 2.49 | 0.04 | 96.18 |
| KH2-443 | 73.65 | 0.29 | 11.60 | 2.44 | 0.09 | 0.24 | 1.57 | 4.08 | 2.54 | 0.07 | 96.57 |
| KH2-443 | 72.87 | 0.29 | 12.03 | 2.45 | 0.07 | 0.22 | 1.58 | 4.42 | 2.55 | 0.07 | 96.56 |
| KH2-443 | 72.53 | 0.29 | 11.05 | 2.30 | 0.10 | 0.23 | 1.67 | 3.65 | 2.48 | 0.05 | 94.35 |
| KH2-446 | 71.47 | 0.27 | 13.16 | 3.73 | 0.16 | 0.15 | 1.24 | 4.93 | 3.39 | 0.04 | 98.53 |
| KH2-446 | 72.31 | 0.07 | 12.23 | 1.01 | 0.04 | 0.07 | 0.65 | 4.06 | 4.25 | 0.01 | 94.70 |
| KH2-446 | 72.91 | 0.07 | 12.46 | 0.91 | 0.07 | 0.06 | 0.80 | 4.11 | 4.17 | 0.01 | 95.58 |
| KH2-446 | 70.52 | 0.27 | 13.26 | 3.78 | 0.14 | 0.21 | 1.30 | 5.30 | 3.50 | 0.04 | 98.31 |
| KH2-446 | 71.58 | 0.26 | 13.36 | 3.82 | 0.16 | 0.21 | 1.30 | 5.30 | 3.61 | 0.04 | 99.64 |
| KH2-446 | 70.70 | 0.28 | 12.90 | 3.71 | 0.14 | 0.22 | 1.25 | 5.06 | 3.57 | 0.03 | 97.85 |
| KH2-446 | 70.87 | 0.26 | 12.65 | 3.84 | 0.13 | 0.18 | 1.20 | 4.96 | 3.42 | 0.03 | 97.56 |
| KH2-446 | 71.71 | 0.07 | 12.34 | 0.99 | 0.04 | 0.08 | 0.73 | 3.74 | 4.58 | 0.02 | 94.31 |

**Appendix C.** Normalised oxide concentrations for ten elements (wt%, mean and SD at 1σ) measured on individual glass shards obtained from Kingshouse 2 Core 2, with total iron expressed as $FeO_t$. For analytical procedures and equipment employed see **Appendix B.5.**

**Appendix D:** Secondary standard measurement results measured at the Oxford University facility using MPI-DING standards GOR132-G, ML38-G and StHs6/80-G (Jochum et al., 2006) and at the Edinburgh University facility using Lipari and BCR2g standards (Kuehn et al., 2011).

| **Standard** | $Na_2O$ | MgO | $Al_2O_3$ | $SiO_2$ | $K_2O$ | CaO | $TiO_2$ | MnO | $FeO_t$ | **Total** |
|---|---|---|---|---|---|---|---|---|---|---|
| GOR132-G | 0.87 | 21.95 | 10.92 | 45.39 | 0.05 | 8.31 | 0.32 | 0.17 | 10.35 | 98.33 |
| GOR132-G | 0.73 | 21.91 | 10.78 | 44.70 | 0.02 | 8.37 | 0.29 | 0.12 | 10.12 | 97.04 |
| GOR132-G | 0.79 | 21.85 | 11.00 | 45.05 | 0.04 | 8.47 | 0.28 | 0.16 | 10.36 | 98.00 |
| GOR132-G | 0.65 | 22.39 | 10.90 | 45.91 | 0.02 | 8.35 | 0.26 | 0.17 | 10.27 | 98.92 |
| GOR132-G | 0.66 | 22.10 | 11.12 | 45.57 | 0.05 | 8.44 | 0.33 | 0.22 | 10.17 | 98.66 |
| GOR132-G | 1.03 | 22.40 | 10.71 | 45.14 | 0.04 | 8.63 | 0.31 | 0.15 | 10.15 | 98.56 |
| ML38-G | 2.29 | 6.44 | 13.78 | 52.01 | 0.39 | 10.55 | 2.06 | 0.15 | 10.93 | 98.60 |
| ML38-G | 2.28 | 6.69 | 13.77 | 52.37 | 0.41 | 10.64 | 2.25 | 0.14 | 11.05 | 99.60 |
| ML38-G | 2.34 | 6.57 | 14.16 | 51.50 | 0.38 | 10.70 | 2.17 | 0.21 | 10.97 | 99.00 |
| ML38-G | 2.25 | 6.59 | 14.05 | 52.02 | 0.37 | 10.61 | 2.18 | 0.19 | 11.23 | 99.49 |
| ML38-G | 2.41 | 6.54 | 13.82 | 51.69 | 0.42 | 10.48 | 2.19 | 0.20 | 10.61 | 98.36 |
| ML38-G | 2.50 | 6.57 | 13.84 | 51.64 | 0.42 | 10.48 | 2.18 | 0.24 | 10.73 | 98.60 |
| ML38-G | 2.22 | 6.58 | 13.78 | 51.54 | 0.36 | 10.54 | 2.22 | 0.22 | 11.05 | 98.51 |
| StHs6/80-G | 4.61 | 1.95 | 17.50 | 63.15 | 1.37 | 5.22 | 0.71 | 0.15 | 4.32 | 98.98 |
| StHs6/80-G | 4.56 | 1.91 | 17.77 | 63.10 | 1.31 | 5.31 | 0.67 | 0.07 | 4.03 | 98.73 |
| StHs6/80-G | 4.85 | 1.85 | 17.45 | 63.16 | 1.31 | 5.14 | 0.76 | 0.01 | 4.57 | 99.10 |
| StHs6/80-G | 4.53 | 1.99 | 17.60 | 63.14 | 1.33 | 5.36 | 0.68 | 0.09 | 4.43 | 99.15 |
| StHs6/80-G | 4.44 | 1.98 | 17.37 | 63.55 | 1.39 | 5.46 | 0.73 | 0.11 | 4.54 | 99.57 |
| StHs6/80-G | 4.82 | 1.84 | 17.72 | 63.92 | 1.32 | 5.41 | 0.69 | 0.10 | 4.32 | 100.14 |

| **Standard** | $Na_2O$ | MgO | $Al_2O_3$ | $SiO_2$ | $K_2O$ | CaO | $TiO_2$ | MnO | $FeO_t$ | $P_2O_5$ | **Total** |
|---|---|---|---|---|---|---|---|---|---|---|---|
| Lipari 5µm | 4.07 | 0.05 | 13.11 | 73.89 | 5.20 | 0.72 | 0.08 | 0.06 | 1.41 | 0.00 | 98.59 |
| Lipari 5µm | 4.12 | 0.04 | 12.72 | 74.81 | 5.13 | 0.79 | 0.08 | 0.05 | 1.59 | 0.01 | 99.34 |
| Lipari 5µm | 4.16 | 0.04 | 12.98 | 74.24 | 5.48 | 0.69 | 0.08 | 0.07 | 1.61 | 0.00 | 99.34 |
| Lipari 5µm | 3.92 | 0.07 | 13.31 | 74.45 | 5.14 | 0.80 | 0.08 | 0.07 | 1.57 | 0.00 | 99.40 |
| BCR2g 5µm | 3.18 | 3.62 | 13.32 | 54.82 | 1.84 | 7.32 | 2.28 | 0.21 | 12.40 | 0.36 | 99.34 |
| BCR2g 5µm | 3.27 | 3.63 | 13.81 | 54.41 | 1.87 | 7.17 | 2.28 | 0.20 | 12.30 | 0.36 | 99.29 |
| BCR2g 5µm | 3.17 | 3.74 | 13.12 | 54.61 | 1.85 | 7.28 | 2.25 | 0.20 | 12.73 | 0.35 | 99.30 |
| BCR2g 5µm | 3.23 | 3.71 | 13.27 | 55.03 | 1.81 | 7.26 | 2.27 | 0.20 | 12.53 | 0.36 | 99.68 |
| BCR2g 5µm | 2.75 | 3.71 | 13.08 | 55.10 | 1.81 | 7.17 | 2.26 | 0.20 | 12.78 | 0.36 | 99.21 |
| BCR2g 5µm | 3.34 | 3.64 | 13.19 | 54.50 | 1.80 | 7.05 | 2.25 | 0.20 | 12.30 | 0.34 | 98.61 |
| BCR2g 5µm | 2.94 | 3.57 | 12.85 | 54.14 | 1.72 | 7.15 | 2.27 | 0.20 | 12.62 | 0.35 | 97.82 |
| BCR2g 5µm | 3.28 | 3.50 | 13.80 | 54.77 | 1.87 | 7.18 | 2.24 | 0.19 | 12.59 | 0.37 | 99.79 |
| Lipari 5µm | 3.70 | 0.03 | 12.74 | 74.59 | 5.23 | 0.71 | 0.07 | 0.07 | 1.41 | -0.01 | 98.54 |
| Lipari 5µm | 4.16 | 0.03 | 12.83 | 74.41 | 5.36 | 0.78 | 0.08 | 0.06 | 1.80 | 0.01 | 99.52 |
| Lipari 5µm | 4.08 | 0.02 | 12.82 | 74.30 | 5.30 | 0.68 | 0.08 | 0.07 | 1.44 | 0.01 | 98.80 |
| Lipari 5µm | 4.11 | 0.03 | 12.32 | 74.25 | 5.18 | 0.71 | 0.08 | 0.07 | 1.55 | 0.00 | 98.31 |
| Lipari 5µm | 3.83 | 0.06 | 13.41 | 74.45 | 5.33 | 0.76 | 0.08 | 0.06 | 1.63 | 0.01 | 99.61 |
| Lipari 5µm | 3.85 | 0.04 | 12.54 | 74.05 | 5.13 | 0.73 | 0.07 | 0.05 | 1.50 | 0.00 | 97.98 |
| Lipari 5µm | 4.34 | 0.02 | 13.70 | 74.27 | 5.16 | 0.78 | 0.08 | 0.08 | 1.58 | 0.01 | 100.01 |
| Lipari 5µm | 4.22 | 0.04 | 13.27 | 74.16 | 5.16 | 0.78 | 0.08 | 0.07 | 1.52 | 0.01 | 99.30 |
| BCR2g 5µm | 3.29 | 3.66 | 13.68 | 54.83 | 1.80 | 7.13 | 2.29 | 0.19 | 12.39 | 0.35 | 99.60 |
| BCR2g 5µm | 3.38 | 3.71 | 13.68 | 54.61 | 1.79 | 7.33 | 2.30 | 0.20 | 12.72 | 0.33 | 100.04 |
| BCR2g 5µm | 3.41 | 3.68 | 13.36 | 55.05 | 1.87 | 7.00 | 2.27 | 0.20 | 12.28 | 0.33 | 99.43 |
| BCR2g 5µm | 3.24 | 3.57 | 13.45 | 54.36 | 1.80 | 7.20 | 2.29 | 0.21 | 11.72 | 0.33 | 98.16 |

| | | | | | | | | | | | |
|---|---|---|---|---|---|---|---|---|---|---|---|
| BCR2g 5µm | 3.05 | 3.62 | 13.10 | 54.50 | 1.82 | 7.08 | 2.29 | 0.19 | 11.92 | 0.31 | 97.89 |
| BCR2g 5µm | 3.33 | 3.53 | 13.61 | 54.47 | 1.81 | 7.18 | 2.29 | 0.21 | 12.65 | 0.32 | 99.39 |
| BCR2g 5µm | 3.22 | 3.52 | 13.72 | 54.31 | 1.82 | 7.33 | 2.29 | 0.19 | 12.16 | 0.32 | 98.89 |
| BCR2g 5µm | 3.19 | 3.57 | 13.20 | 54.37 | 1.78 | 7.29 | 2.30 | 0.20 | 12.47 | 0.31 | 98.67 |
| BCR2g 5µm | 3.21 | 3.62 | 13.24 | 54.02 | 1.79 | 7.28 | 2.31 | 0.22 | 12.47 | 0.32 | 98.47 |
| BCR2g 5µm | 3.40 | 3.75 | 13.71 | 54.12 | 1.75 | 7.27 | 2.29 | 0.20 | 12.80 | 0.32 | 99.59 |
| Lipari 5µm | 4.14 | 0.03 | 12.86 | 74.48 | 5.23 | 0.59 | 0.07 | 0.07 | 5.23 | 0.01 | 99.07 |
| Lipari 5µm | 4.23 | 0.04 | 13.03 | 75.40 | 5.02 | 0.74 | 0.07 | 0.06 | 5.02 | 0.00 | 100.02 |
| Lipari 5µm | 4.14 | 0.04 | 12.91 | 74.79 | 5.31 | 0.71 | 0.08 | 0.07 | 5.31 | 0.01 | 99.32 |
| Lipari 5µm | 4.19 | 0.04 | 13.11 | 74.23 | 5.10 | 0.77 | 0.07 | 0.07 | 5.10 | 0.01 | 99.17 |
| Lipari 5µm | 3.96 | 0.01 | 12.88 | 74.33 | 5.27 | 0.69 | 0.08 | 0.08 | 5.27 | 0.01 | 98.65 |
| Lipari 5µm | 4.16 | 0.05 | 12.87 | 74.64 | 5.07 | 0.73 | 0.08 | 0.07 | 5.07 | 0.01 | 99.22 |
| Lipari 5µm | 4.21 | 0.05 | 13.16 | 74.27 | 5.15 | 0.77 | 0.08 | 0.07 | 5.15 | 0.00 | 99.25 |
| Lipari 5µm | 4.01 | 0.01 | 12.77 | 73.32 | 5.03 | 0.73 | 0.08 | 0.07 | 5.03 | 0.00 | 97.25 |
| Lipari 5µm | 4.05 | 0.06 | 12.65 | 73.82 | 5.18 | 0.85 | 0.08 | 0.06 | 5.18 | 0.00 | 98.21 |
| Lipari 5µm | 4.26 | 0.06 | 12.92 | 74.48 | 5.23 | 0.75 | 0.08 | 0.06 | 5.23 | 0.01 | 99.66 |
| | | | | | | | | | | | |
| Lipari 3µm | 0.18 | 0.03 | 13.48 | 79.27 | 1.97 | 0.78 | 0.07 | 0.08 | 1.62 | 0.01 | 97.49 |
| Lipari 3µm | 4.33 | 0.06 | 13.30 | 74.62 | 5.16 | 0.77 | 0.08 | 0.06 | 1.39 | 0.01 | 99.77 |
| Lipari 3µm | 4.49 | 0.06 | 13.58 | 74.30 | 5.34 | 0.76 | 0.08 | 0.07 | 1.59 | 0.01 | 100.26 |
| Lipari 3µm | 3.75 | 0.01 | 11.91 | 74.35 | 5.21 | 0.74 | 0.08 | 0.07 | 1.63 | 0.01 | 97.76 |
| Lipari 3µm | 4.02 | 0.03 | 12.51 | 74.36 | 5.26 | 0.77 | 0.07 | 0.05 | 1.46 | 0.01 | 98.53 |
| Lipari 3µm | 3.87 | 0.01 | 12.86 | 73.23 | 5.12 | 0.75 | 0.07 | 0.06 | 1.52 | 0.01 | 97.51 |
| Lipari 3µm | 3.90 | 0.03 | 13.11 | 73.11 | 5.29 | 0.75 | 0.08 | 0.07 | 1.81 | 0.01 | 98.16 |
| Lipari 3µm | 3.73 | 0.03 | 13.46 | 73.84 | 5.22 | 0.72 | 0.08 | 0.07 | 1.58 | 0.01 | 98.72 |
| Lipari 3µm | 4.23 | 0.02 | 12.73 | 73.80 | 5.17 | 0.77 | 0.08 | 0.08 | 1.55 | 0.01 | 98.44 |
| Lipari 3µm | 4.07 | 0.01 | 12.54 | 74.45 | 5.26 | 0.77 | 0.07 | 0.07 | 1.56 | 0.01 | 98.82 |
| BCR2g 3µm | 2.87 | 3.69 | 12.46 | 55.55 | 1.87 | 7.13 | 2.26 | 0.20 | 12.79 | 0.31 | 99.13 |
| BCR2g 3µm | 3.01 | 3.58 | 12.16 | 54.77 | 1.85 | 7.34 | 2.27 | 0.19 | 12.21 | 0.33 | 97.71 |
| BCR2g 3µm | 3.48 | 3.75 | 13.77 | 54.92 | 1.75 | 7.27 | 2.28 | 0.21 | 12.54 | 0.33 | 100.29 |
| BCR2g 3µm | 2.95 | 3.59 | 14.01 | 54.75 | 1.79 | 7.23 | 2.26 | 0.18 | 12.37 | 0.32 | 99.45 |
| BCR2g 3µm | 3.27 | 3.62 | 14.49 | 54.61 | 1.74 | 7.03 | 2.26 | 0.19 | 12.58 | 0.32 | 100.10 |
| BCR2g 3µm | 4.02 | 3.66 | 13.07 | 54.68 | 1.79 | 7.14 | 2.28 | 0.21 | 12.88 | 0.33 | 100.06 |
| BCR2g 3µm | 3.50 | 3.64 | 14.48 | 54.51 | 1.84 | 6.97 | 2.26 | 0.20 | 12.88 | 0.32 | 100.60 |
| BCR2g 3µm | 3.52 | 3.66 | 14.15 | 54.52 | 1.86 | 7.10 | 2.28 | 0.20 | 12.18 | 0.33 | 99.77 |
| BCR2g 3µm | 3.25 | 3.74 | 13.74 | 54.74 | 1.82 | 7.12 | 2.25 | 0.21 | 12.78 | 0.33 | 99.98 |
| BCR2g 3µm | 3.38 | 3.48 | 13.63 | 55.35 | 1.79 | 7.23 | 2.28 | 0.20 | 12.31 | 0.35 | 100.01 |

**Appendix E:** Preferred Bayesian P_sequence age-depth model coding for the Kingshouse 2 basal sediment sequence produced using OxCal version 4.3 (Bronk Ramsey and Lee, 2013), the IntCal13 calibration curve (Reimer et al., 2013) and applying the age estimate for the Askja-S Tephra of Kearney et al. (2018).

```
Options()
 {
  Resolution=1;
  kIterations=100;
 };
 Plot()
 {
  Outlier_Model("General", T(5), U(0,4), "t");
  P_Sequence("Kingshouse 2", 1, 1, U(-2,2))
  {
   Boundary("KH2 470cm")
   {
    z=470;
    color="Gray";
   };
   Date("KH2 467cm")
   {
    z=467;
   };
   Date("KH2 466cm")
   {
    z=466;
   };
   Date("KH2 464cm")
   {
    z=464;
   };
   Date("KH2 463cm")
   {
    z=463;
   };
   Date("KH2 462cm")
   {
    z=462;
   };
   Date("KH2 460cm")
   {
    z=460;
   };
   Date("KH2 451cm")
   {
    z=451;
   };
   Date("KH2 450cm")
   {
    z=450;
   };
   Date("KH2 443.5cm")
   {
    z=443.5;
   };
   Date("KH2 442.5cm")
   {
    z=442.5;
   };
   Date("KH2 432cm")
   {
    z=432;
   };
```

```
 Boundary("Top of litho-unit 5b (KH2 430cm)")
 {
  z=430;
  color="Gray";
 };
};
Sequence("KH2 466-467cm")
{
 Boundary("=KH2 467cm");
 Delta_R("Moss 466-467cm", U(0, 500));
 R_Date("OxA-32471 (KH2 466-467)", 10015, 45)
 {
  Outlier("General",0.05);
  z=466.5;
  color="Blue";
 };
 Boundary("=KH2 466cm");
};
Sequence("KH2 463-464cm")
{
 Boundary("=KH2 464cm");
 Date("Abernethy Tephra (KH2 463-464cm)", N(calBP(11462), 122))
 {
  z=463.5;
  color="Brown";
 };
 Boundary("=KH2 463cm");
};
Sequence("KH2 462-464cm")
{
 Boundary("=KH2 464cm");
 Phase("462-464cm")
 {
  Delta_R("Moss 462-464cm", U(0, 500));
  R_Date("OxA-35408 (KH2 462-464)", 9915, 45)
  {
   z=463;
   Outlier("General", 0.05);
   color="Blue";
  };
  Delta_R("=None");
  R_Date("OxA-35409 (KH2 462-464)", 9860, 50)
  {
   z=463;
   Outlier("General", 0.05);
   color="Green";
  };
 };
 Boundary("=KH2 462cm");
};
Sequence("KH2 462-463cm")
{
 Boundary("=KH2 463cm");
 Delta_R("None", 0);
 R_Date("OxA-32470 (KH2 462-463)", 9870, 40)
 {
  z=463.5;
  Outlier("General", 0.05);
  color="Green";
 };
 Boundary("=KH2 462cm");
};
Sequence("KH2 460-462cm")
{
 Boundary("=KH2 462cm");
 Phase("460-462cm")
 {
```

```
  Delta_R("Moss 460-462cm", U(0, 500));
  R_Date("OxA-35410 (KH2 462-460)", 9920, 60)
  {
   z=461;
   Outlier("General", 0.05);
   color="Blue";
  };
  Delta_R("=None");
  R_Date("OxA-35411 (KH2 462-460)", 9825, 45)
  {
   z=461;
   Outlier("General", 0.05);
   color="Green";
  };
 };
 Boundary("=KH2 460cm");
};
Sequence("KH2 450-451cm")
{
 Boundary("=KH2 451cm");
 Delta_R("Moss 450-451cm", U(0, 500));
 R_Date("OxA-32469 (KH2 450-451)", 9935, 45)
 {
  Outlier("General", 0.05);
  z=450.5;
  color="Blue";
 };
 Boundary("=KH2 450cm");
};
Sequence("KH2 442.5-443.5cm")
{
 Boundary("=KH2 443.5cm");
 Date("Askja-S Tephra (KH2 442.5-443.5", N(calBP(10824),49))
 {
  z=443;
  color="Brown";
 };
 Boundary("=KH2 442.5cm");
};
Sequence("KH2 430-432cm")
{
 Boundary("=KH2 432cm");
 Delta_R("=None");
 R_Date("OxA-35596 (KH2 430-432)", 9146, 39)
 {
  Outlier("General", 0.05);
  z=431;
  color="Green";
 };
 Boundary("=Top of litho-unit 5b (KH2 430cm)");
};
};
```

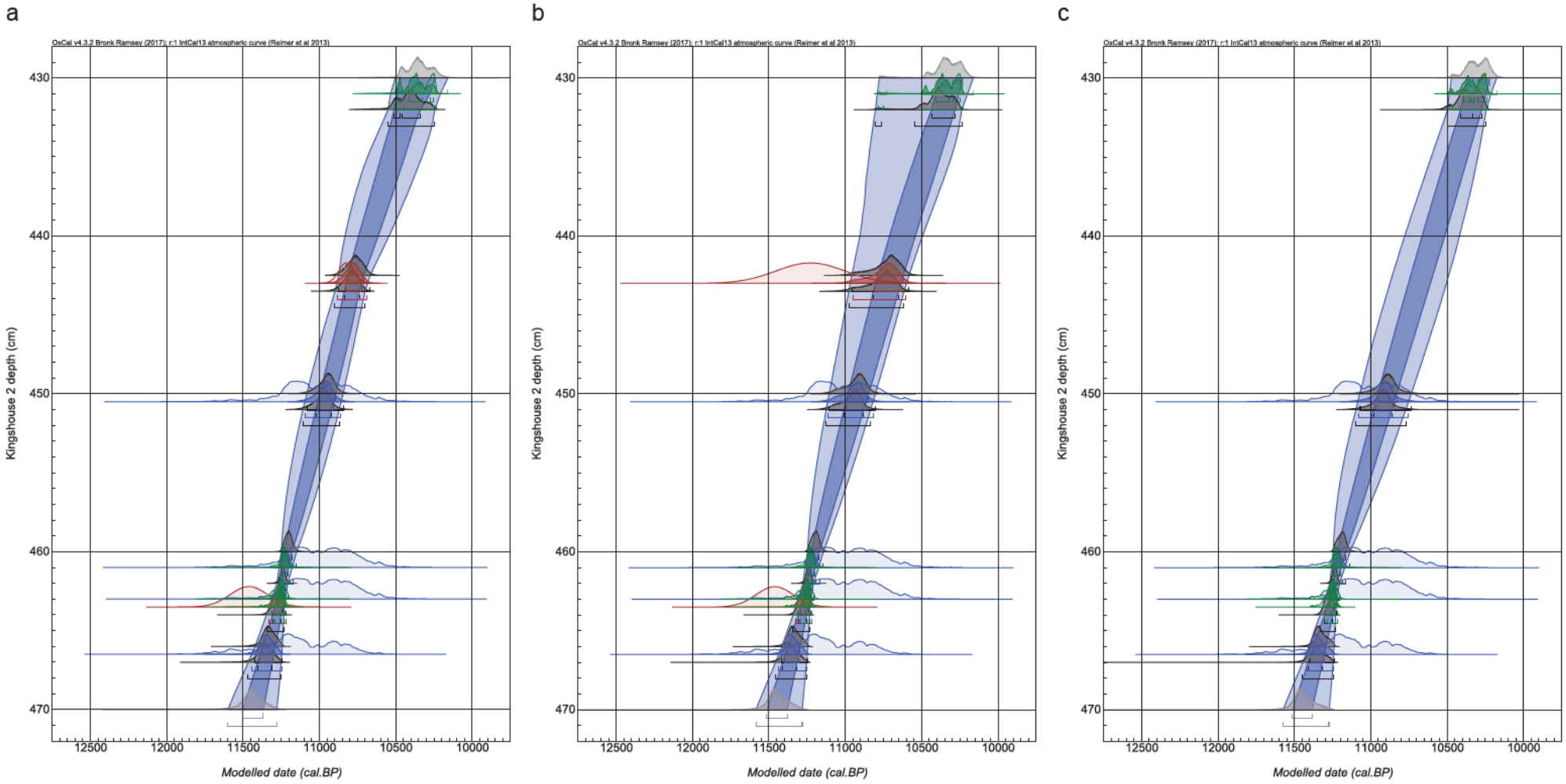


**Appendix F.** Bayesian 'P_Sequence' age-depth models for the Kingshouse 2 basal sediment sequence produced using OxCal version 4.3 (Bronk Ramsey and Lee, 2013) and the IntCal13 calibration curve (Reimer et al., 2013): **A.** Incorporating the Askja-S Tephra age estimate of Kearney et al., 2018. **B.** Incorporating the Askja-S Tephra age estimate of Ott et al., 2016. **C.** based on radiocarbon dates only. Light blue and dark blue shading show the limits of the 95.4% and 68% probability ranges respectively.

| Core reference | Sample reference | Sample weight (mg) | Core depth (m) | Dated material | Radiocarbon age (yr) | Weighted mean cal. age |
|---|---|---|---|---|---|---|
| RM-10-1A | OS-89748 | 3.4 | 6.28-6.30 | *Betula* twig | 9960 ± 50 | 11,419 ± 116 |
| | OS-84280 | 5.3 | 6.68-6.70 | *Sphagnum*, unidentified leaf fragments | 10,100 ± 45 | 11,695 ± 141 |
| | OS-93723 | 3.0 | 6.98-7.0 | Beetle | 10,100 ± 35 | 11,701 ± 123 |
| RM-10-1C | OS-84215 | 5.0 | 5.00-5.01 | *Vaccinium* leaf fragment, unidentified stem | 9940 ± 55 | 11,395 ± 115 |
| | OS-84320 | 3.0 | 5.03-5.04 | *Pogonatum*, unidentified leaf fragments | 10,200 ± 80 | 11,885 ± 176 |
| RM-10-1D | OS-89837 | 3.0 | 4.93-4.94 | *Sphagnum, Potamogeton, Betula* leaf | 9980 ± 50 | 11,453 ± 119 |
| RM-10-3A | OS-99979 | 3.1 | 4.92-4.93 | *Sphagnum* | 9740 ± 40 | 11,176 ± 54 |
| | OS-99978* | 5.0 | 4.96-4.97 | *Empetrum* seed, *Pogonatum*, unidentified stem | 10,350 ± 40 | 12,217 ± 103 |
| | OS-89842* | 3.1 | 4.96-4.97 | *Sphagnum, Pogonatum*, unidentified leaf fragments | 10,500 ± 50 | 12,446 ± 100 |
| | OS-89841* | 3.0 | 4.99-5.00 | *Chara, Nitella, Potamogeton, Empetrum* seed | 10,300 ± 70 | 12,120 ± 158 |
| | OS-99977* | 5.0 | 4.99-5.00 | *Empetrum* seed, *Pogonatum* | 10,400 ± 45 | 12,274 ± 105 |
| RM-12-1 | OS-100114 | 5.0 | 6.88-6.89 | *Chara, Nitella, Potamogeton, Sphagnum* | 9970 ± 65 | 11,456 ± 135 |
| | 112593 | 5.4 | 6.90-6.92 | *Potamogeton, Pogonatum*, unidentified stems | 10,040 ± 40 | 11,547 ± 115 |
| RM-12-2A | 112596 | 18.9 | 4.68-4.70 | *Rhacomitrium* | 9870 ± 20 | 11,256 ± 20 |
| | 112595 | 16.8 | 4.73-4.74 | *Sphagnum*, unidentified leaf fragments | 9935 ± 20 | 11,318 ± 43 |
| | OS-99684 | 18.9 | 4.74-4.77 | *Sphagnum, Pogonatum, Potamogeton* | 10,050 ± 65 | 11,583 ± 158 |
| RM-12-2B | 112599 | 7.4 | 4.64-4.66 | *Rhacomitrium, Pogonatum,* wood fragment | 9920 ± 20 | 11,300 ± 35 |
| | 112598 | 5.4 | 4.69-4.71 | *Rhacomitrium, Pogonatum, Empetrum* seed, unidentified bud | 9945 ± 20 | 11,332 ± 52 |
| RM-12-3A | 112601 | 7.2 | 4.93-4.94 | *Pogonatum, Sphagnum, Betula* leaf fragments | 10,090 ± 130 | 11,687 ± 245 |
| | OS-99685 | 5.2 | 4.95-4.97 | *Pogonatum*, wood fragment, *Betula* leaf fragment | 10,550 ± 65 | 12,481 ± 95 |
| RM-12-3B | 112603* | 6.0 | 4.89-4.90 | *Pogonatum, Vaccinium* leaf fragments | 10,120 ± 170 | 11,760 ± 303 |
| | OS-100115* | 6.4 | 4.90-4.92 | Unidentified leaf fragments | 10,100 ± 70 | 11,685 ± 174 |
| RM-12-4A | 112605* | 31.0 | 5.40-5.41 | *Rhacomitrium* | 9990 ± 20 | 11,449 ± 91 |
| | 112604* | 22.2 | 5.41-5.44 | *Rhacomitrium* | 9965 ± 20 | 11,375 ± 77 |
| RM-12-4B | 112607 | 3.8 | 5.36-5.38 | *Rhacomitrium* | 10,040 ± 35 | 11.544 ± 107 |
| | OS-99686 | 7.4 | 5.4-5.41 | *Rhacomitrium* | 10,050 ± 60 | 11,579 ± 151 |
| RM-12-5 | 112609 | 2.7 | 4.78-4.8 | *Empetrum* seed*, Nitella, Betuala* leaf fragments | 8910 ± 60 | 10,024 ± 110 |
| | 112608 | 2.4 | 4.8-4.81 | *Nitella, Chara, Betula* seed*, Sphagnum,* unidentified seeds | 9140 ± 180 | 10,319 ± 267 |
| RM-13-3 | OS-104751 | 21 | 3.93-3.94 | *Rhacomitrium* | 9860 ± 35 | 11,258 ± 33 |
| | OS-10478* | 13 | 4.01-4.02 | *Rhacomitrium* | 10,150 ± 35 | 11,836 ± 95 |
| | OS-104747* | 10 | 4.08-4.09 | *Rhacomitrium* | 10,100 ± 40 | 11,698 ± 133 |
| 191 | OS-104746* | 12 | 4.08-4.09 | *Rhacomitrium* | 10,250 ± 85 | 11,999 ± 191 |

**Appendix G.** Radiocarbon dates obtained from basal deposits in basins on Rannoch Moor published by Bromley et al. (2014).